NACA

RESEARCH MEMORANDUM

INVESTIGATION OF PERFORMANCE OF SINGLE-STAGE AXIAL-FLOW COMPRESSOR USING NACA 5509-34 BLADE SECTION

By Harry Mankuta and Donald C. Guentert

Lewis Flight Propulsion Laboratory
Cleveland, Ohio

TECHNICAL EDITING WAIVED

NATIONAL ADVISORY COMMITTEE FOR AERONAUTICS

WASHINGTON
September 30, 1948

NACA RM No. E8F30

NATIONAL ADVISORY COMMITTEE FOR AERONAUTICS

RESEARCH MEMORANDUM

INVESTIGATION OF PERFORMANCE OF SINGLE-STAGE AXIAL-FLOW COMPRESSOR USING NACA 5509-34 BLADE SECTION

By Harry Mankuta and Donald C. Guentert

SUMMARY

An investigation was conducted to study the performance of a single-stage axial-flow compressor using blades with an NACA 5509-34 airfoil section. The compressor had a 14-inch tip diameter with a hub-to-tip diameter ratio of 0.8 at the entrance to the rotor. Static- and total-pressure, total-temperature, and flow-angle surveys were taken in the compressor inlet and outlet and between blade rows to study both the over-all performance and individual blade-row performance.

The performance of the rotor and stator blade rows is presented separately on the basis of three different measures of blade loading: turning angle, lift coefficient, and a loading factor defined as the ratio of the change in tangential velocity through the blades to the mean axial velocity. Discrepancies between the weight flow as measured by the orifice and the weight flow obtained by a mechanical integration of the axial-flow components across the passage at the various measuring stations indicated a need for more complete and precise instrumentation between the blade rows.

The over-all performance results at design speed showed that a maximum total-pressure ratio of 1.262 and a maximum adiabatic efficiency of 0.84 were obtained at an equivalent weight flow of 10.50 pounds per second.

INTRODUCTION

Axial-flow compressor research is currently aimed at obtaining information that will permit the design of axial-flow compressors with high pressure rise per stage without sacrifice of

efficiency or flow capacity. One phase of the research program is the development and investigation of various airfoil sections in two-dimensional and three-dimensional cascades for the purpose of obtaining information concerning blade loading and its limitations. Information of this nature is essential in the design of compressors that are to operate with a maximum pressure rise and high efficiency. Because of radial pressure gradients and flows set up by centrifugal forces, however, and because of the possible effects due to adjacent blade rows, the flow in an actual compressor is much more complex than that encountered in cascade investigations. Blade performance must therefore be investigated under actual compressor operating conditions in order to determine the effect of these additional variables. Because of the complexities introduced in the investigation of a multistage compressor, it is desirable to perform the investigation on a single-stage compressor consisting of an initial set of guide vanes followed by a set of rotor and a set of stator blades.

A 14-inch-diameter compressor of this type has been used at the NACA Cleveland laboratory to investigate the effect of different blade sections on compressor performance. The hub-to-tip diameter ratio of this compressor was 0.8 in order to be representative of the usual dimensions of the middle stages of a multistage compressor. The first set of blades investigated in this unit used the NACA 5509-34 airfoil section and was similar to the blades used in the fourth stage of the NACA eight-stage compressor (reference 1). A design procedure similar to that of reference 1, which had the same solidity and Mach number limitations, was used.

In order to obtain complete information concerning flow characteristics and individual blade-row performance in a single-stage compressor, it is necessary to take pressure and temperature measurements between the blade rows. Because of the very limited space available between the blade rows, difficulty was encountered in obtaining instruments sufficiently small to fit between the blade rows without sacrificing accuracy. In addition, the proximity of adjacent blade rows to the measuring plane very probably has an effect upon the pressure and angle measurements. Radial flows and pressure gradients also complicate the instrumentation. The problem of instrumentation was therefore important in the investigation of the first blade design.

This investigation was conducted over a wide range of air flows at corrected rotor speeds of 7265, 11,500, and 14,530 rpm, corresponding to approximately one-half, three-quarters, and full design speed, respectively. The over-all performance is presented

as plots of total-pressure ratio and adiabatic efficiency against corrected weight flow. The individual blade-row performance is studied on the basis of three loading parameters: turning angle, lift coefficient, and a loading factor defined as the ratio of the change in tangential velocity through the blades to the mean axial velocity.

994

SYMBOLS

The following symbols are used in this report:

C_L	lift coefficient
c_p	specific heat at constant pressure, Btu/(lb)($^\circ$F)
g	acceleration due to gravity, 32.174,(ft/sec^2)
H_{ad}	adiabatic work input per pound, (ft-lb/lb)
H_M	actual work input per pound calculated from increase in angular momentum across rotor,(ft-lb/lb)
H_T	actual work input per pound calculated from total-temperature rise, (ft-lb/lb)
J	mechanical equivalent of heat, 778, (ft-lb/Btu)
K	constant in turning-angle relation
N	rotor speed, (rpm)
$N/\sqrt{\theta}$	rotor speed corrected to standard sea-level temperature, (rpm)
P	total pressure, (lb/sq ft absolute)
p	static pressure, (lb/sq ft absolute)
r	radius to blade element, (ft)
T	total temperature, ($^\circ$R)
t	static temperature, ($^\circ$R)
U	velocity of blade ωr at radius r, (ft/sec)

V	absolute air velocity, (ft/sec)
V'	air velocity relative to rotor, (ft/sec)
W	weight flow rate, (lb/sec)
$W\sqrt{\theta/\delta}$	weight flow rate corrected to standard sea-level pressure and temperature, (lb/sec)
α	angle of attack, (deg)
α_0	angle of attack of isolated airfoil for zero lift, (deg)
β	absolute stagger angle, angle between compressor axis and absolute air velocity, (deg)
β'	relative stagger angle, angle between compressor axis and air velocity relative to rotor, (deg)
γ	ratio of specific heats (c_p/c_v)
$\Delta\beta$	turning angle (stator), (deg)
$\Delta\beta'$	turning angle (rotor), (deg)
δ	ratio of inlet total pressure to standard sea-level pressure
η_{ad}	adiabatic efficiency of compressor
θ	ratio of inlet total temperature to standard sea-level temperature
ρ	density, (slugs/cu ft)
σ	blade-element solidity, ratio of chord length to distance between adjacent blades
ω	absolute angular velocity of blade, (radians/sec)

Subscripts:

0	inlet depression tank
1	inlet to rotor
2	inlet to stator

3	outlet of stator
av	average
e	referred to equivalent constant axial-velocity diagram
h	hub
m	referred to vector-mean velocity
t	tip
z	axial
θ	tangential

COMPRESSOR DESIGN

Aerodynamic. - The first blade design to be investigated in the 14-inch variable-component axial-flow compressor rig was designed with a radial distribution of velocity and pressure, aerodynamic limitation, and flow assumptions that were similar to those used in the design of the fourth stage of the NACA eight-stage compressor (reference 1).

In this design procedure, a design velocity diagram was set up in which the velocities were expressed as ratios of the tip speed. In setting up this diagram, the following conditions were assumed:

1. Constant tip diameter

2. Ratio of hub-to-tip diameter at inlet to rotor blades equal to 0.8

3. Ratio of axial velocity at hub to tip speed at inlet to rotor equal to 0.6 (selected to provide maximum power input for hub-to-tip ratio of 0.8)

4. Vortex-type rotation added by rotor blades; value of change in tangential component at hub set by σC_L limitation of 0.77; rotation added by rotor blades removed by stator blades

5. Symmetrical diagram at hub of rotor

6. Wheel-type rotation added by inlet guide vanes; value of tangential component added by guide vanes at hub determined by requirement of symmetrical diagram

7. Constant total enthalpy and no radial component of flow assumed in calculating variation of axial velocity across passage entering and leaving each blade row; value of axial velocity component entering stator blades at hub determined by setting Mach number at hub on stator blades equal to Mach number at hub on preceding rotor blades

8. Passage height at each station determined by continuity requirement, with compression process assumed to be isentropic

Actual velocities were obtained by setting the Mach number of the maximum air velocity relative to the blades equal to 0.7.

Cascade data were unavailable on the NACA 5509-34 airfoil. The following relation, taken from reference 2, was therefore used to determine the blade-angle settings necessary to produce the required turning angles.

$$\theta = K(\alpha - \alpha_0)$$

The value of K was taken as 0.9, and a value of -5.6° obtained from interpolation of isolated-airfoil tests, was used for the angle of attack at zero lift α_0.

The NACA 5509-34 blade section was used for both rotor and stator blades, which were of constant section across the passage. The coordinates of the NACA 5509-34 blade section are presented in table I. The guide vanes were formed with circular arc surfaces faired into an elliptical nose section. Information concerning design turning angles and angles of attack for this blade design are given in the following table:

Blade row	Radius (in.)	Design stagger angle (deg)	Design turning angle (deg)	Design angle of attack (deg)
Guide vanes: 40 blades	Tip - 7.00	0	31.61	--------
	a - 6.82	0	30.45	--------
	b - 6.47	0	28.36	--------
	c - 6.11	0	26.33	--------
	d - 5.76	0	24.43	--------
	Hub - 5.60 (rotor leading edge)	0	23.58	--------
NACA 5509-34 airfoil section: rotor; 29 blades	Tip - 7.00	51.71	9.36	4.80
	a - 6.82	50.45	10.44	6.00
	b - 6.47	48.01	12.56	8.38
	c - 6.11	45.50	14.75	10.80
	d - 5.76	43.04	16.87	13.17
	Hub - 5.60 (rotor leading edge)	41.93	17.85	14.25
NACA 5509-34 airfoil section: stator; 30 blades	Tip - 7.00	47.81	17.25	13.56
	a - 6.84	46.75	17.04	13.32
	b - 6.51	44.87	16.72	13.03
	c - 6.18	43.21	16.60	12.91
	d - 5.85	41.81	16.71	13.00
	Hub - 5.70 (stator leading edge)	41.21	16.85	13.12

Mechanical. - The mechanical features of the compressor are shown in figure 1. The compressor had a constant tip diameter of 14.00 inches and a hub diameter that varied from 11.20 inches at the leading edge of the rotor blade to 11.72 inches at the trailing edge of the stator blade. The axial distance between the trailing edge of one set of blades and the leading edge of the following set was approximately 0.5 inch. The clearance between the rotor-blade tips and the compressor casing was 0.020 inch, whereas, the clearance between the stator blades and the compressor hub was 0.010 inch. Three spherically seated journal bearings and a fixed-wedge-type thrust bearing were used on the rotor shaft. A set of exit turning vanes was located approximately 7 chord lengths downstream of the stator blades. These turning vanes were designed to remove the remaining whirl component of the air

with its resulting radial pressure gradient before discharge into the collector. An annular baffle was provided in the collector to aid in providing a uniform flow around its periphery.

APPARATUS AND METHODS

Apparatus

A sketch of the compressor setup is shown in figure 2. Two 225-horsepower dynamometers mounted in tandem were used to drive the compressor throught a 7.25:1 speed increaser. Air was taken in directly from the room through a thin-plate orifice mounted in an orifice tank and then passed through a motor-operated throttle valve into a large depression tank. This tank was 4 feet in diameter, 6 feet long, and contained a felt filter and a 3-by-3-inch honeycomb to aid in producing a smooth flow at the compressor inlet. The tank sufficiently reduced the inlet-air velocities that the compressor-inlet pressure and temperature measurements made in the tank could be assumed to be stagnation values. A bellmouth inlet was used to provide a smooth flow from the tank into the compressor-inlet guide vanes. The compressor-discharge collector was connected to the laboratory exhaust system through two exhaust pipes. A motor-driven throttle valve was provided in the exhaust system to vary the flow through the compressor.

Instrumentation

Instrumentation was provided at the compressor inlet and outlet to measure over-all compressor performance and between blade rows to measure individual blade-row performance. The four instrument stations are shown in figure 1. All measurements at stations 1, 2, and 3 were taken at four radial positions across the flow passage. All instruments were circumferentially located in such a manner as to be removed from the wakes of upstream blades or instruments.

Station 0 was located in the inlet depression tank. Because of the size of this tank, the small existing velocities were neglected, and pressure and temperature measurements were assumed to be stagnation values. Temperatures in the inlet depression tank were measured by four thermocouple probes, each containing four thermocouples. Two wall pressure taps were used for pressure measurement.

Stations 1 and 2 were located approximately 1/5 chord length before and after the rotor, respectively. The total temperature was

assumed to be constant across the guide vanes and across the stator blades, so no temperatures were measured at stations 1 and 2. Total pressures at each station were obtained with a single total-pressure rake similar to that shown in figure 3(a). The variation in flow angle from hub to tip at a given flow was considered to be sufficiently small to permit the orientation of the rake in the direction of the flow in the center of the passage with negligible effect on the accuracy of the total-pressure measurements at the other radial positions. Because of the limited space existing between the blade rows, a special type of miniature static-pressure survey tube (fig. 3(b)) was designed. These tubes were individually calibrated with respect to Mach number. A single radial static-pressure survey of four points was taken with one of these tubes at stations 1 and 2. The orientation of all static-pressure tubes with the flow yaw angle was accomplished by balancing the pressures obtained from separate static-pressure taps on each side of the instrument.

In addition, three wall static taps in the outside wall were used. Flow-angle measurements at each station were obtained from a single radial survey with a claw tube similar to that shown in figure 3(c).

Compressor-outlet measurements were made at station 3, which was located approximately 1 chord length downstream of the stator blades. Total-temperature measurements were obtained from four rakes containing four probe thermocouples each (fig. 3(d)). In order to permit the measurement of the energy addition to the air by means of the rise in total temperature across the compressor, a high degree of accuracy in the measurement of the total-temperature rise is required. For this reason, the thermocouples in the rakes at station 3 were connected differentially with those at station 0 in such a manner as to measure a circumferentially averaged value of the temperature rise across the compressor at each of the four radii located by the four probes on each rake. Total-pressure measurements were obtained from four 19-tube circumferential total-pressure rakes (fig. 3(e)) distributed around the periphery of the compressor. Each of these rakes was located at a different radial position and was connected differentially to the inlet depression tank to give a measurement of the total-pressure rise across the compressor at each of four radii.

Static pressure at station 3 was obtained from a single radial survey taken with a Prandtl type static-pressure tube shown in figure 3(f). In addition, three wall static-pressure taps were provided in both the outside and inside wall. Flow angles were obtained by means of a single radial survey with a claw tube similar to that used at stations 1 and 2.

Airflow through the compressor was measured by a standard thin-plate intake orifice mounted in an orifice tank. Compressor speed was measured within ±10 rpm with a precision-type tachometer.

A summary of the instrumentation used in the investigation is presented in the following table:

Station	Radial measuring positions (in.)	Measurement	Instrument	Circumferential positions
Station 0, inlet tank	---	Total pressure	Wall tap	2
		Total temperature	Thermocouple probe	4
Station 1, after guide vanes	a - 6.82 b - 6.47 c - 6.11 d - 5.76	Total pressure	Radial total-pressure rake	1
		Static pressure	Miniature static-pressure survey	1
			Wall tap, outside wall	3
		Yaw angle	Claw survey tube	1
Station 2, after rotor	a - 6.84 b - 6.51 c - 6.18 d - 5.85	Total pressure	Radial total-pressure rake	1
		Static pressure	Miniature static-pressure survey tube	1
			Wall tap, outside wall	3
		Yaw angle	Claw survey tube	1
Station 3, after stator	a - 6.86 b - 6.57 c - 6.29 d - 6.00	Total pressure	Circumferential total-pressure rake	4
		Static pressure	Static-pressure survey tube	1
			Wall tap, inside wall	3
			Wall tap, outside wall	3
		Total temperature	Thermocouple rake	4
		Yaw angle	Claw survey tube	1

Accuracy of Measurements

Over-all performance measurements. - The accuracy with which the over-all performance of the compressor may be expressed in terms of total-pressure ratio and adiabatic efficiency depends primarily upon the accuracy of the total-pressure measurements at stations 0 and 3 and upon the measurement of the total-temperature rise between these two stations. The method used in measuring the total pressure at stations 0 and 3 permits an accuracy within approximately ±1 percent of the dynamic head. In order to obtain the total-temperature rise across the compressor, a recovery coefficient based on an average calibration curve of a group of thermocouple probes was applied to the observed temperature readings. Differences between the recovery coefficient of individual thermocouples and the average calibration curve due to small differences in the construction may introduce a small error in the temperature readings. An oil coating from bearing-oil leakage into the air stream may also change the thermocouple recovery coefficient sufficiently to introduce an error in the temperature measurements. When these sources of errors are considered, it is estimated that the measurements of temperature rise across the compressor are accurate to within approximately ±3 percent of the stagnation temperature rise.

Blade-row-performance measurements. - The problem of obtaining air-flow measurements between the blade rows was complicated by space limitations. At the closest points, the space between blade rows, was approximately 1/2 inch, which means that the actual measurements were taken within less than 1/4 chord length of the blades. This space limitation not only necessitated the use of very small pressure tubes with their attendant difficulties, but also increased the possibility of an effect upon the measurements by the flow disturbances generated by the blades.

As a check on the accuracy of this instrumentation, the weight flows obtained by integrating the quantity $2\pi\rho g V_z r dr$ across the passage at stations 1, 2, and 3 were compared with the weight flow measured by the orifice. The percentage discrepancy between the integrated weight flows at each station and the orifice measured weight flow are plotted as a function of weight flow in figure 4.

The variation in the error in integrated weight flow at station 1 with changes in flow for three speeds are presented in figure 4(a). At this station, all the integrated weight flows were within ±4 percent of the orifice measured flows. No definite relation seems to exist between the error in weight flow and the weight flow as measured by the orifice.

The variation in the error in integrated weight flow at station 2 with changes in flow at the same three speeds are presented in figure 4(b). At this station, the integrated weight flows vary from about 4 percent above the orifice-measured weight flow to approximately 7 percent below.

The variation in the error in integrated weight flow at station 3 with changes in flow at the three speeds are presented in figure 4(c). At most points at this station, the integrated weight flow was higher than the orifice-measured weight flow. The error in weight flow varied from approximately 13 to approximately -3 percent. In general, the difference between the integrated weight flow and the orifice measured weight flow decreased with increasing weight flow.

Possible causes for the large discrepancies between integrated weight flows and the weight flow measured by the orifice may be divided into three general categories: (1) differences between the flow conditions prevailing in the compressor and the uniform flow existing in the tunnel in which the instruments were calibrated, which made the calibrations invalid, (2) existence of unmeasured radial-flow components, and (3) circumferential-flow variations that may invalidate the application of measurements made at a single circumferential position to the entire periphery of the compressor.

Calibrations of all pressure-measuring instruments were obtained under uniform steady-flow conditions. In the compressor, these ideal-flow conditions do not exist and the calibration therefore may not be entirely accurate. Immediately downstream of the rotor (station 2), a fluctuating flow due to the wakes produced by the rotor blades undoubtedly exists. Because the total-pressure instruments under fluctuating-flow conditions measure the root-mean-square value of the velocity fluctuation rather than the average value, an error is introduced. It is possible that these flow fluctuations will also affect the accuracy of the static-pressure measurements.

Another flow condition that may cause an error in the static-pressure measurements is the presence of radial components of flow. A sufficiently large component of flow across the short dimension of the static-pressure tubes may cause an appreciable error in the static-pressure measurement. The actual magnitude of this error is unknown, however, as no measurements were made of flow pitch angle (angle between the flow direction and the compressor axis in a plane through the axis and the measuring point). Another error tending to

cause a discrepancy between integrated weight flow and orifice measured weight flow is introduced by the presence of radial components of flow inasmuch as the velocities calculated from the pressure measurements were assumed to have no radial component. This error is small, however, as a pitch angle of 10° causes an approximate error of only 1.5 percent in the axial velocity.

Circumferential variations in flow may be either a periodic symmetrical variation produced by the pressure fields or wakes set up by the stationary blades, or an unsymmetrical variation around the periphery of the compressor. With the exception of the circumferential total-pressure rakes used at station 3, all flow-measurement surveys were made at a single circumferential position. An error is obviously introduced if the flow conditions at this point do not represent an average condition. Although this possible error could not be evaluated, it is probably a primary factor in producing the discrepancies between the integrated weight flows and the weight flow as measured by the orifice.

The magnitude of the discrepancies existing between the integrated weight flows at the various measuring stations and the weight flow measured by the orifice makes it apparent that any individual blade-row performance results must be treated with caution. If these discrepancies are to be reduced in future investigations, it appears that circumferential surveys of all flow measurements must be made in order to detect and account for circumferential-flow variations produced by individual blades. In addition, it is probably advisable to provide some means for detecting unsymmetrical flow variations that may exist around the compressor periphery. Some provision for the measurement of flow pitch angle also appears to be desirable.

Methods of Investigation

During the investigation, the absolute pressure in the inlet tank was maintained at 25 inches of mercury by throttling through the inlet valve. The weight flow was varied in approximately equal increments by varying the compressor back pressure with the outlet throttle. Runs were made at corrected rotor speeds $N/\sqrt{\theta}$ of 7265, 11,500, and 14,530 rpm, corresponding to approximately one-half, three-quarters, and full design speed, respectively. The range of Reynolds numbers covered during the investigation, based on blade chord, was approximately 250,000 to 500,000, and the Mach number of the flow relative to the blades varied from approximately 0.2 to 0.76.

Methods of Rating

Total-pressure ratio. - The total-pressure ratio used in this investigation is the average pressure ratio that would be obtained with an isentropic power input to the measured total air flow equal to the actual isentropic power input integrated over the flow passage. It is calculated by means of a mechanical integration of the following equation

$$\left(\frac{P_3}{P_0}\right)_{av} = \left\{ \frac{\int_{r_{h,3}}^{r_{t,3}} \left[\left(\frac{P_3}{P_0}\right)^{\frac{\gamma-1}{\gamma}} - 1 \right] \rho_3 V_{z,3} r dr}{\int_{r_{h,3}}^{r_{t,3}} \rho_3 V_{z,3} r dr} + 1 \right\}^{\frac{\gamma}{\gamma-1}}$$

Adiabatic efficiency. - The adiabatic efficiency used in evaluating the compressor performance is based on the total-temperature rise across the compressor and is defined by the equation

$$\eta_{ad} = \frac{H_{ad}}{H_T}$$

The adiabatic work input per pound of air is H_{ad} and is calculated from the equation

$$H_{ad} = Jc_p T_0 \left[\left(\frac{P_3}{P_0}\right)_{av}^{\frac{\gamma-1}{\gamma}} - 1 \right]$$

The actual work input per pound of air, as measured by the total-temperature rise across the compressor, is H_T. It is obtained from a mechanical integration of the following equation:

$$H_T = \frac{Jc_p \int_{r_{h,3}}^{r_{t,3}} \left(T_3 - T_0\right) \rho_3 V_{z,3} r dr}{\int_{r_{h,3}}^{r_{t,3}} \rho_3 V_{z,3} r dr}$$

Another method that was available to calculate the actual work input involves the determination of the change in angular momentum of the flow across the rotor. This quantity can be obtained from the equation

$$H_M = \frac{\omega}{g}\left[\left(\frac{\int_{r_{h,2}}^{r_{t,2}} V_{\theta,2}\rho_2 V_{z,2} r^2 dr}{\int_{r_{h,2}}^{r_{t,2}} \rho_2 V_{z,2} r dr}\right) - \left(\frac{\int_{r_{h,1}}^{r_{t,1}} V_{\theta,1}\rho_1 V_{z,1} r^2 dr}{\int_{r_{h,1}}^{r_{t,1}} \rho_1 V_{z,1} r dr}\right)\right]$$

A comparison of the work input determined by this method with the work input calculated from the total-temperature rise is shown in figure 5. In most cases, H_M is lower than H_T. The maximum difference between the curves varies from approximately 22 percent at design speed to approximately 16 percent at one-half design speed.

Because of the previously noted discrepancies between the integrated weight flows using the flow measurements at the various measuring stations and the orifice measured weight flows, H_M was not considered to be as accurate as H_T. For this reason, the efficiencies were calculated on a total-temperature-rise basis.

RESULTS AND DISCUSSION

The data obtained at the three rotor speeds are presented in table II.

Over-all Performance

The over-all performance of the compressor is presented in figure 6 as curves of total-pressure ratio and adiabatic temperature-rise efficiency against equivalent weight flow.

At design speed, a peak total-pressure ratio of 1.262 was obtained at an efficiency of 0.84 and an equivalent weight flow of 10.50 pounds per second. Design value for the total-pressure ratio was 1.210 at an equivalent weight flow of 13.45 pounds per second, based on an isentropic compression process. Because of restrictions in the exhaust system, the maximum corrected weight flow obtained during the performance tests was 13.25 pounds per second. With an efficiency of 0.71 obtained by extrapolating the efficiency curve to the design weight flow, the design pressure ratio would be 1.146 as compared to an actual value of 1.140 obtained by extrapolating the pressure-ratio curve to the design weight flow.

The peak adiabatic temperature-rise efficiency at design speed was 0.84 and was obtained at approximately the same weight flow for which the maximum pressure ratio was obtained. The peak efficiency increased to 0.92 at one-half design speed (7265 rpm). These efficiencies were obtained with interstage instrumentation in place. Check runs made with this instrumentation removed showed an increase in efficiency varying between 1 and 3 percent over the upper half of the flow range at the three speeds.

When the absolute values of the adiabatic temperature-rise efficiency are considered, it should be remembered that these values are based on a power input determined from a measurement of the total-temperature rise across the compressor. Because the temperature rise across a single-stage axial-flow compressor is small, of the order of magnitude of the stagnation-temperature rise, a small error in the temperature measurement may introduce an appreciable error in the efficiency.

Blade-Row Performance

Pressure rise in a blade row is a function of turning imparted to the air, or blade loading. The performance of rotor and stator

blade rows is presented in figures 7 to 9 on the basis of three different measures of blade loading. In figures 7(a) and 7(b), a plot of turning angle against angle of attack is presented for the rotor and stator, respectively. For this plot, an equivalent constant axial-velocity diagram, (shown with dotted lines in fig. 10) was used to obtain values of turning angle and angle of attack. This method is the method used in reference 3 to obtain correlation between turning angles obtained in a variable axial-velocity three-dimensional cascade and turning angles obtained in a constant axial-velocity two-dimensional cascade.

Curves are plotted in figures 7 to 9 for four different radii at three speeds. The effect of speed on the turning angle appears to be very small. It should be noted that because the variation in angle of attack was obtained by varying the flow, the air stagger angle did not remain constant. Any effect of the air stagger angle on turning angle will therefore also appear in these curves. Reference 4 indicates that the value of K in the expression $\theta = K(\alpha - \alpha_0)$ varies appreciably with changes in stagger angle and solidity.

The design point at each radius is also indicated. At the design angle of attack on the rotor, the measured turning angle at all radial positions except d were within 1° of the design turning angle predicted by the equation

$$\theta = 0.9\ (\alpha - \alpha_0)$$

For the stator blades, the design turning angles were within 3° of the measured turning angles with the exception of the radial position near the hub where the measured turning angle was 7° lower than the design value.

Curves of σC_L against an entering-air angle of attack based on the velocity vectors V'_1 and V_2 (fig. 10) for the rotor and stator are plotted in figures 8(a) and 8(b), respectively. Drag forces were neglected in calculating the values of σC_L and the lift force was assumed to be normal to the mean relative velocity vectors V'_m and V_m for the rotor and the stator, respectively. The values of σC_L were calculated from the equations

$$\sigma C_L = \frac{2\Delta V'_\theta}{V'_m} \quad \text{(rotor)}$$

$$\sigma C_L = \frac{2\Delta V_\theta}{V_m} \quad \text{(stator)}$$

In figures 9(a) and 9(b) are plotted curves of a loading factor $\Delta V'_\theta/V'_{z,m}$ against $V'_{\theta,m}/V'_{z,m}$ for the rotor and of $\Delta V_\theta/V_{z,m}$ against $V_{\theta,m}/V_{z,m}$ for the stator.

SUMMARY OF RESULTS

As a result of the investigation conducted to study the performance of a single-stage axial-flow compressor using blades with an NACA 5509-34 airfoil section, the following results were obtained:

1. At design speed, a maximum total-pressure ratio of 1.262 and a maximum adiabatic efficiency of 0.84 were obtained at an equivalent weight flow of 10.50 pounds per second.

2. The measured turning angles across the rotor at all radial positions except near the hub were within 1° of the design turning angles at the design angles of attack. For the stator blades, the design turning angles were within 3° of the measured turning angles with the exception of the radial position near the hub where the measured turning angle was 7° lower than the design value.

Lewis Flight Propulsion Laboratory,
National Advisory Committee for Aeronautics,
Cleveland, Ohio.

REFERENCES

1. Sinnette, John T., Schey, Oscar W., and King, J. Austin: Performance of NACA Eight-Stage Axial-Flow Compressor Designed on the Basis of Airfoil Theory. NACA Rep. No. 758, 1944.

2. Kantrowitz, Arthur, and Daum, Fred L.: Preliminary Experimental Investigation of Airfoils in Cascade. NACA CB, July 1942.

3. Bogdonoff, Seymour M., and Herrig, L. Joseph: Performance of Axial-Flow Fan and Compressor Blades Designed for High Loadings. NACA TN No. 1201, 1947.

4. Bogdonoff, Seymour M., and Hess, Eugene E.: Axial-Flow Fan and Compressor Blade Design Data at 52.5° Stagger and Further Verification of Cascade Data by Rotor Tests. NACA TN No. 1271, 1947.

TABLE 1. - SECTION COORDINATES OF NACA 5509-34 BLADE SECTION

UPPER SURFACE		LOWER SURFACE	
X	Y	X	Y
0.00	0.00	0.00	0.00
1.03	1.23	1.47	-.41
2.21	1.96	2.79	-.49
4.64	3.13	5.36	-.54
7.10	4.11	7.90	-.52
9.58	4.94	10.42	-.47
14.58	6.36	15.42	-.33
19.61	7.45	20.39	-.15
29.73	8.95	30.27	.27
39.88	9.68	40.12	.69
50.04	9.76	49.96	1.02
60.19	9.23	59.81	1.26
70.30	8.05	69.70	1.35
80.38	6.13	79.62	1.20
90.28	3.31	89.72	.56
95.16	1.68	94.84	.18
100.00	.09	100.00	-.09

TABLE II - SUMMARY OF PERFORMANCE DATA OF 14-INCH SINGLE-STAGE AXIAL-FLOW COMPRESSOR USING NACA 5509-34 BLADE SECTION

		Station 0		Station 1							Station 2							Station 3					
Equivalent weight flow (orifice) $W\sqrt{\theta}/\delta$ (lb/sec)	Radial position	Pressure $p = P$ (in. Hg abs.)	Temperature $t = T$ (°R)	Radius (in.)	Actual blade speed (ft/sec)	Total pressure P (in. Hg abs.)	Static pressure p (in. Hg abs.)	Total temperature, T (°R)	Flow angle β_1 (deg)	Absolute air velocity (ft/sec)	Radius (in.)	Actual blade speed (ft/sec)	Total pressure P (in. Hg abs.)	Static pressure p (in. Hg abs.)	Total temperature, T (°R)	Flow angle β_2 (deg)	Absolute air velocity (ft/sec)	Radius (in.)	Total pressure P (in. Hg abs.)	Static pressure p (in. Hg abs.)	Total temperature, T (°R)	Flow angle β_3 (deg)	Absolute air velocity (ft/sec)
Equivalent rotor speed, 14,530 rpm (design)																							
13.25	a	24.88	542.2	5.82	682.8	24.82	20.44	542.2	26.25	693.7	6.84	886.9	29.42	22.87	572.9	41.75	692.3	6.96	28.43	22.22	572.9	26.00	665.0
	b			6.47	637.7	24.82	20.29		25.25	667.8	6.51	843.9	29.05	22.56	574.0	40.75	718.1	6.57	28.27	22.09	574.0	26.00	731.4
	c			6.11	792.6	24.85	20.18		24.25	618.0	6.18	802.0	29.62	22.46	571.9	39.25	784.5	6.29	28.25	21.95	571.9	23.50	795.9
	d			5.76	746.0	24.89	19.91		22.75	617.9	5.85	758.4	28.84	22.21	572.7	37.75	696.1	6.00	27.97	21.90	572.7	22.50	678.7
11.28	a	25.00	545.4	5.82	685.6	24.90	22.07	545.4	24.75	472.1	6.84	888.7	31.11	26.46	550.9	49.25	888.5	6.95	31.25	27.00	550.9	29.50	587.6
	b			6.47	640.4	24.99	21.94		24.75	490.5	6.51	848.6	31.85	26.53	588.4	47.75	801.6	6.57	31.67	26.92	588.4	26.50	667.0
	c			6.11	795.2	24.99	21.78		24.75	503.6	6.18	804.5	31.45	26.33	587.6	47.25	791.7	6.29	31.41	26.80	587.6	25.50	660.4
	d			5.76	748.4	24.62	21.71		22.75	497.4	5.85	760.9	31.54	26.18	588.5	46.75	607.1	6.00	30.09	26.71	588.5	30.00	619.0
10.42	a	25.00	548.4	5.82	686.0	24.94	22.05	545.4	24.75	432.4	6.84	889.2	32.11	27.15	554.1	54.96	662.2	6.95	31.50	27.72	554.1	31.50	606.4
	b			6.47	640.8	24.99	22.33		24.75	455.7	6.51	847.0	32.41	27.22	558.8	52.25	698.6	6.57	31.97	27.71	558.8	30.50	633.9
	c			6.11	795.6	24.99	22.21		24.75	457.3	6.18	804.9	31.99	27.07	556.5	49.75	575.9	6.29	31.84	27.64	556.5	28.50	650.7
	d			5.76	748.8	24.84	22.15		22.75	460.6	5.85	761.2	32.02	26.98	550.7	48.75	595.0	6.00	31.13	27.54	550.7	28.00	496.5
9.52	a	25.00	544.3	5.82	682.8	24.96	23.04	544.3	25.25	395.7	6.84	888.9	32.37	27.12	554.1	66.45	662.5	6.95	30.95	27.60	554.1	30.00	454.7
	b			6.47	637.7	24.99	22.88		25.25	404.3	6.51	849.9	32.45	27.21	558.5	63.25	691.8	6.57	31.30	27.72	558.5	31.00	492.3
	c			6.11	792.6	24.99	22.76		24.25	415.5	6.18	802.0	33.52	27.22	550.1	60.75	594.5	6.29	31.89	27.52	550.1	29.50	524.6
	d			5.76	746.0	24.84	22.63		22.25	416.3	5.85	758.4	32.27	27.10	558.2	49.25	588.5	6.00	31.06	27.59	558.2	31.00	490.2
8.72	a	25.00	549.1	5.82	683.9	24.96	23.42	543.1	24.75	342.9	6.84	887.0	32.16	26.87	555.4	72.75	659.9	6.95	30.49	27.72	555.4	29.50	438.1
	b			6.47	638.8	24.97	23.26		24.75	353.3	6.51	845.0	32.09	26.99	551.9	66.25	692.5	6.57	30.74	27.58	551.8	30.50	469.4
	c			6.11	793.6	24.99	23.12		24.25	379.9	6.18	803.0	32.55	27.00	559.6	60.95	607.6	6.29	31.18	27.46	559.6	30.50	502.6
	d			5.76	747.0	24.80	22.95		22.25	378.7	5.85	759.4	32.31	27.05	559.3	49.25	592.4	6.00	30.71	27.47	559.3	35.50	473.3
8.44	a	25.00	543.4	5.82	683.9	24.96	23.54	543.4	24.75	329.1	6.84	887.0	30.43	25.65	556.2	70.75	654.1	6.95	30.18	27.64	556.2	28.50	420.5
	b			6.47	638.8	24.99	23.38		24.75	351.4	6.51	845.0	31.68	26.66	556.4	67.55	686.8	6.57	30.36	27.47	556.4	31.00	449.5
	c			6.11	793.6	25.00	23.24		24.25	367.4	6.18	803.0	32.59	26.90	551.2	61.75	617.5	6.29	30.94	27.33	551.2	30.50	498.2
	d			5.76	747.0	24.87	23.08		21.75	373.0	5.85	759.4	32.43	26.96	550.0	49.25	603.7	6.00	30.47	27.34	550.0	39.50	454.8
8.10	a	25.00	543.4	5.82	683.9	24.95	23.70	543.4	24.75	308.2	6.84	887.0	30.82	25.65	555.9	74.25	648.2	6.95	30.01	27.58	555.9	28.50	414.0
	b			6.47	638.8	24.98	23.50		24.75	337.1	6.51	845.0	31.66	26.59	553.1	69.75	590.5	6.57	30.27	27.41	553.1	31.00	448.6
	c			6.11	793.6	25.00	23.35		24.25	355.7	6.18	803.0	32.65	26.81	550.6	61.25	628.8	6.29	30.78	27.33	550.6	31.25	457.4
	d			5.76	747.0	24.88	23.21		21.75	358.6	5.85	759.4	32.45	26.93	550.7	48.25	608.1	6.00	30.24	27.35	550.7	39.00	449.8
7.72	a	25.00	543.0	5.82	683.9	24.93	23.79	543.0	24.75	295.9	6.84	887.0	31.12	25.54	556.5	77.75	667.3	6.95	29.93	27.59	556.5	29.00	407.7
	b			6.47	638.8	24.99	23.62		24.75	323.0	6.51	845.0	31.69	26.55	556.0	64.75	687.4	6.57	30.03	27.36	556.0	31.50	432.3
	c			6.11	793.6	24.99	23.49		24.25	338.2	6.18	803.0	32.44	26.76	551.8	61.75	617.7	6.29	30.83	27.29	551.8	32.00	475.0
	d			5.76	747.0	24.90	23.35		22.25	345.0	5.85	759.4	32.39	26.93	552.4	47.75	606.2	6.00	29.94	27.32	552.4	39.50	429.6
Equivalent rotor speed, 11,000 rpm																							
11.63	a	25.00	543.9	5.82	700.2	24.83	21.86	543.9	23.25	484.4	6.84	702.7	26.46	22.82	557.5	35.75	551.9	6.86	28.27	21.93	557.5	28.50	588.1
	b			6.47	654.4	24.97	21.72		24.25	506.8	6.51	669.4	27.11	22.24	557.4	36.45	608.3	6.57	28.81	21.76	557.4	25.00	623.6
	c			6.11	629.7	24.98	21.71		24.75	508.3	6.18	636.1	27.32	22.09	557.7	35.25	630.0	6.29	28.69	21.66	557.7	23.50	634.3
	d			5.76	691.7	24.88	21.83		20.00	516.9	5.85	601.6	26.93	21.91	559.0	34.25	621.0	6.00	28.66	21.54	559.0	26.00	626.8
10.93	a	25.00	546.0	5.82	700.6	24.90	22.35	546.0	24.75	447.2	6.84	703.1	27.67	23.91	565.8	41.25	541.3	6.96	27.48	22.72	565.8	26.00	559.4
	b			6.47	654.8	24.99	22.21		24.75	466.8	6.51	669.8	28.09	23.71	559.9	41.25	570.5	6.57	27.88	22.66	559.9	26.00	562.0
	c			6.11	629.1	25.00	22.13		24.25	473.7	6.18	636.5	28.04	23.51	555.1	40.25	579.1	6.29	27.86	22.56	555.1	24.00	555.8
	d			5.76	592.1	24.81	21.98		22.75	473.7	5.85	601.9	27.63	23.31	555.1	38.75	588.1	6.00	27.14	22.44	555.1	25.50	529.1
10.32	a	25.00	544.2	5.82	700.2	24.90	22.67	544.2	24.25	418.1	6.84	702.7	26.25	24.80	556.4	43.75	515.7	6.96	28.05	24.70	556.4	27.00	494.6
	b			6.47	654.4	24.99	22.65		24.25	439.8	6.51	669.4	26.49	24.43	556.1	42.75	542.4	6.57	28.27	24.67	556.1	25.50	511.6
	c			6.11	629.7	24.99	22.47		24.25	442.8	6.18	636.1	26.38	24.43	556.1	42.45	585.6	6.29	28.25	24.68	556.1	25.00	518.4
	d			5.76	691.7	24.87	22.37		22.75	448.8	5.85	601.6	26.05	24.19	556.2	40.75	532.8	6.00	27.81	24.48	556.2	31.00	471.9

8.99	a	25.00	546.5	6.82	700.6	24.97	22.79	546.5	24.75	410.8	6.84	703.1	28.09	25.01	570.8	45.25	473.7	6.86	28.52	26.10	570.8	28.00	496.3
	b			6.47	664.8	24.99	22.45		25.25	428.6	6.51	669.9	28.69	24.89	570.7	44.25	535.0	6.57	28.05	25.03	570.7	27.60	511.1
	c			6.11	629.1	24.99	22.59		24.25	432.7	6.18	636.5	28.73	24.99	568.9	44.25	536.2	6.29	28.46	24.97	568.9	28.50	502.2
	d			5.76	592.1	24.83	22.49		18.75	429.5	5.85	601.9	28.39	24.85	569.2	42.75	527.9	6.00	27.95	24.89	569.2	31.50	473.1
8.65	a	25.00	545.0	6.82	700.2	24.89	23.43	545.0	23.75	337.5	6.84	702.7	28.11	25.40	569.7	46.45	443.8	6.86	28.67	25.61	569.7	28.00	457.9
	b			6.47	664.4	24.98	22.91		25.05	399.8	6.51	669.4	28.06	25.37	569.5	45.45	512.3	6.57	28.21	25.25	569.5	27.25	480.2
	c			6.11	628.7	24.96	22.79		23.75	412.1	6.18	636.1	28.80	25.20	568.0	44.75	506.7	6.29	28.55	25.50	568.0	28.00	466.4
	d			5.76	591.7	24.79	22.71		22.25	402.2	5.85	601.6	28.54	25.02	568.3	43.75	503.5	6.00	28.11	25.43	568.3	31.50	439.3
8.92	a	25.00	546.1	6.82	700.2	24.93	23.28	546.1	24.25	367.5	6.84	702.7	28.52	25.84	573.8	50.25	450.2	6.86	28.75	26.19	573.8	28.00	427.1
	b			6.47	664.4	24.98	23.14		24.75	376.4	6.51	669.4	29.13	25.69	571.8	47.45	477.8	6.57	29.02	26.13	571.8	28.25	452.1
	c			6.11	628.7	24.99	23.10		24.25	383.1	6.18	636.1	29.04	25.79	571.8	47.25	479.6	6.29	28.95	26.11	571.3	28.00	449.2
	d			5.76	591.7	24.82	23.05		22.75	374.0	5.85	601.6	29.06	25.71	572.9	46.25	496.9	6.00	28.85	26.02	572.9	31.05	432.8
8.26	a	25.00	545.4	6.82	700.2	24.91	23.88	545.4	24.75	321.4	6.84	702.7	28.97	26.19	575.1	56.75	443.8	6.86	28.91	26.69	575.1	30.80	395.4
	b			6.47	664.4	24.99	23.44		24.75	344.8	6.51	669.4	29.14	26.19	572.9	48.75	456.4	6.57	29.13	26.66	572.9	28.50	416.4
	c			6.11	628.7	24.99	23.41		24.25	347.6	6.18	636.1	29.28	26.20	572.4	48.75	453.7	6.29	29.14	26.58	572.4	28.00	422.3
	d			5.76	591.7	24.82	23.33		22.75	350.0	5.85	601.6	29.31	26.21	574.1	46.25	498.2	6.00	28.84	26.52	574.1	31.50	408.1
7.87	a	25.00	545.4	6.82	700.2	24.91	23.95	545.4	24.75	293.5	6.84	702.7	29.36	26.21	577.2	66.26	470.9	6.86	28.74	26.76	577.2	29.20	375.0
	b			6.47	664.4	24.99	23.80		24.75	301.7	6.51	669.4	29.44	26.19	572.8	51.25	476.4	6.57	29.03	26.71	572.8	29.85	403.5
	c			6.11	628.7	24.99	23.64		24.25	321.4	6.18	636.1	29.69	26.22	574.2	50.45	491.1	6.29	29.17	26.64	574.2	30.55	421.1
	d			5.76	591.7	24.83	23.54		22.75	326.8	5.85	601.6	29.56	26.22	574.8	49.25	494.3	6.00	28.96	26.61	574.8	32.00	406.3
7.03	a	25.00	545.2	6.82	700.2	24.92	24.09	545.2	25.25	250.7	6.84	702.7	29.87	26.00	576.0	70.75	456.5	6.86	28.45	26.74	576.0	28.00	350.0
	b			6.47	664.4	24.99	23.92		25.25	235.5	6.51	669.4	29.29	25.84	575.6	56.45	488.2	6.57	28.90	26.63	575.6	30.60	408.7
	c			6.11	628.7	24.99	23.81		24.25	238.6	6.18	636.1	29.73	26.04	576.0	51.75	506.5	6.29	28.96	26.59	575.0	30.55	410.7
	d			5.76	591.7	24.86	23.75		22.75	304.6	5.85	601.6	29.60	26.11	574.1	49.75	494.4	6.00	28.73	26.50	574.1	32.00	388.1
Equivalent rotor speed, 7,255 rpm																							
8.27	a	24.92	541.9	6.82	440.1	24.88	23.40	541.9	24.25	330.5	6.84	441.5	28.23	23.44	546.4	32.25	390.2	6.86	28.19	23.03	546.4	23.80	409.0
	b			6.47	417.6	24.90	23.37		24.75	341.7	6.51	420.7	25.51	23.35	547.0	32.75	405.9	6.57	28.43	22.98	547.0	24.00	434.7
	c			6.11	396.1	24.90	23.30		24.25	340.9	6.18	399.8	25.66	23.31	546.7	31.75	421.3	6.29	28.45	22.96	546.7	23.80	437.3
	d			5.76	371.9	24.85	23.26		22.25	349.5	5.85	378.1	26.42	23.26	547.2	32.25	406.8	6.00	28.40	22.95	547.2	26.00	434.0
7.41	a	25.01	543.0	6.82	441.7	24.95	23.85	543.0	24.25	299.3	6.84	443.3	28.99	24.30	550.0	39.75	343.9	6.86	28.87	24.11	550.0	24.80	363.6
	b			6.47	419.2	25.00	23.77		24.25	306.9	6.51	422.3	26.10	24.22	550.5	39.25	373.3	6.57	26.01	24.07	550.5	25.50	382.4
	c			6.11	396.6	25.00	23.74		24.25	309.5	6.18	401.3	26.14	24.18	549.9	37.95	393.0	6.29	25.93	24.06	549.9	23.00	384.4
	d			5.76	373.3	24.97	23.67		22.25	315.4	5.85	378.5	26.99	24.11	549.9	37.25	375.3	6.00	25.79	24.01	549.9	24.50	365.0
6.85	a	24.99	542.9	6.82	441.9	24.95	23.99	542.9	24.75	270.5	6.84	443.5	28.14	24.69	551.1	42.25	339.7	6.86	28.17	24.52	551.1	26.85	339.2
	b			6.47	419.4	24.99	23.93		24.25	282.9	6.51	422.5	26.89	24.66	551.9	42.25	352.0	6.57	26.27	24.51	551.9	26.00	352.0
	c			6.11	396.8	24.99	23.91		24.25	285.0	6.18	401.5	26.82	24.65	551.0	41.25	349.3	6.29	26.23	24.59	551.0	24.50	351.8
	d			5.76	373.5	24.83	23.87		22.25	288.0	5.85	379.7	26.19	24.57	551.0	40.25	346.7	6.00	26.03	24.53	551.0	28.00	334.0
6.36	a	24.99	543.8	6.82	442.4	24.91	24.11	543.8	24.25	248.1	6.84	444.0	28.28	24.99	553.4	44.96	303.9	6.86	28.40	25.05	553.4	27.50	315.7
	b			6.47	419.8	24.98	24.07		24.25	253.7	6.51	422.9	26.82	24.96	553.6	44.75	340.1	6.57	26.46	24.85	553.6	25.50	345.1
	c			6.11	397.2	24.99	24.04		23.25	257.1	6.18	401.9	26.49	24.90	552.0	43.95	342.0	6.29	26.42	24.95	552.0	24.00	320.8
	d			5.76	373.9	24.95	23.99		22.25	270.2	5.85	380.1	26.37	24.84	552.5	42.75	336.9	6.00	26.29	24.92	552.5	31.00	312.3
5.76	a	25.00	543.3	6.82	441.9	25.04	24.31	543.3	24.75	234.9	6.84	443.5	28.30	25.24	553.9	48.25	279.4	6.86	28.45	25.41	553.9	27.50	276.3
	b			6.47	419.4	24.99	24.26		24.25	234.9	6.51	422.5	26.84	25.39	553.4	46.75	300.9	6.57	26.88	25.39	553.4	26.50	282.0
	c			6.11	396.8	24.99	24.24		23.75	238.7	6.18	401.5	26.62	25.29	553.0	46.75	312.6	6.29	26.56	25.35	553.0	24.50	294.9
	d			5.76	373.5	24.97	24.19		22.25	242.9	5.85	379.7	26.59	25.29	553.8	46.25	307.1	6.00	26.43	25.30	553.8	30.50	282.0
5.01	a	25.00	543.5	6.82	441.9	24.91	24.47	543.5	24.25	182.4	6.84	443.5	28.59	25.53	555.5	59.75	279.9	6.86	28.65	25.68	555.5	30.50	262.4
	b			6.47	419.4	24.98	24.43		24.25	201.5	6.51	422.5	26.74	25.55	554.8	49.25	295.4	6.57	26.63	25.67	554.8	29.00	266.4
	c			6.11	396.8	24.98	24.39		23.25	214.6	6.18	401.5	26.77	25.52	554.5	49.25	301.2	6.29	26.65	25.67	554.5	29.00	266.2
	d			5.76	373.5	24.96	24.36		22.25	214.6	5.85	379.7	26.77	25.54	554.6	49.25	298.3	6.00	26.56	25.51	554.6	35.50	262.9
4.68	a	24.99	543.8	6.82	441.5	24.95	24.67	543.8	24.55	166.9	6.84	443.1	28.76	25.80	557.0	66.26	301.6	6.86	28.82	25.71	557.0	28.00	245.3
	b			6.47	419.0	24.99	24.55		24.55	182.5	6.51	422.1	26.76	25.61	555.8	51.75	301.6	6.57	26.67	25.66	555.8	29.20	256.0
	c			6.11	396.4	24.98	24.48		23.75	197.1	6.18	401.1	26.83	25.61	555.2	50.75	310.3	6.29	26.63	25.59	555.2	30.00	258.0
	d			5.76	373.1	24.98	24.44		22.25	201.5	5.85	379.3	26.82	25.53	555.2	50.25	307.5	6.00	26.55	25.50	555.2	35.50	242.3
4.38	a	25.00	543.5	6.82	441.9	24.93	24.62	543.5	24.75	155.3	6.84	443.5	28.50	25.49	555.7	72.25	292.9	6.86	28.43	25.39	555.7	28.50	233.6
	b			6.47	419.4	24.99	24.59		24.75	177.3	6.51	422.5	26.72	25.41	555.0	56.75	310.5	6.57	26.60	25.35	555.0	30.00	248.9
	c			6.11	396.8	24.99	24.54		23.75	182.5	6.18	401.5	26.82	25.46	555.3	51.25	313.1	6.29	26.56	25.38	555.3	30.50	250.9
	d			5.76	373.5	24.96	24.50		22.25	187.6	5.85	379.7	26.84	25.48	555.4	49.75	313.1	6.00	26.50	25.34	555.4	37.50	232.4

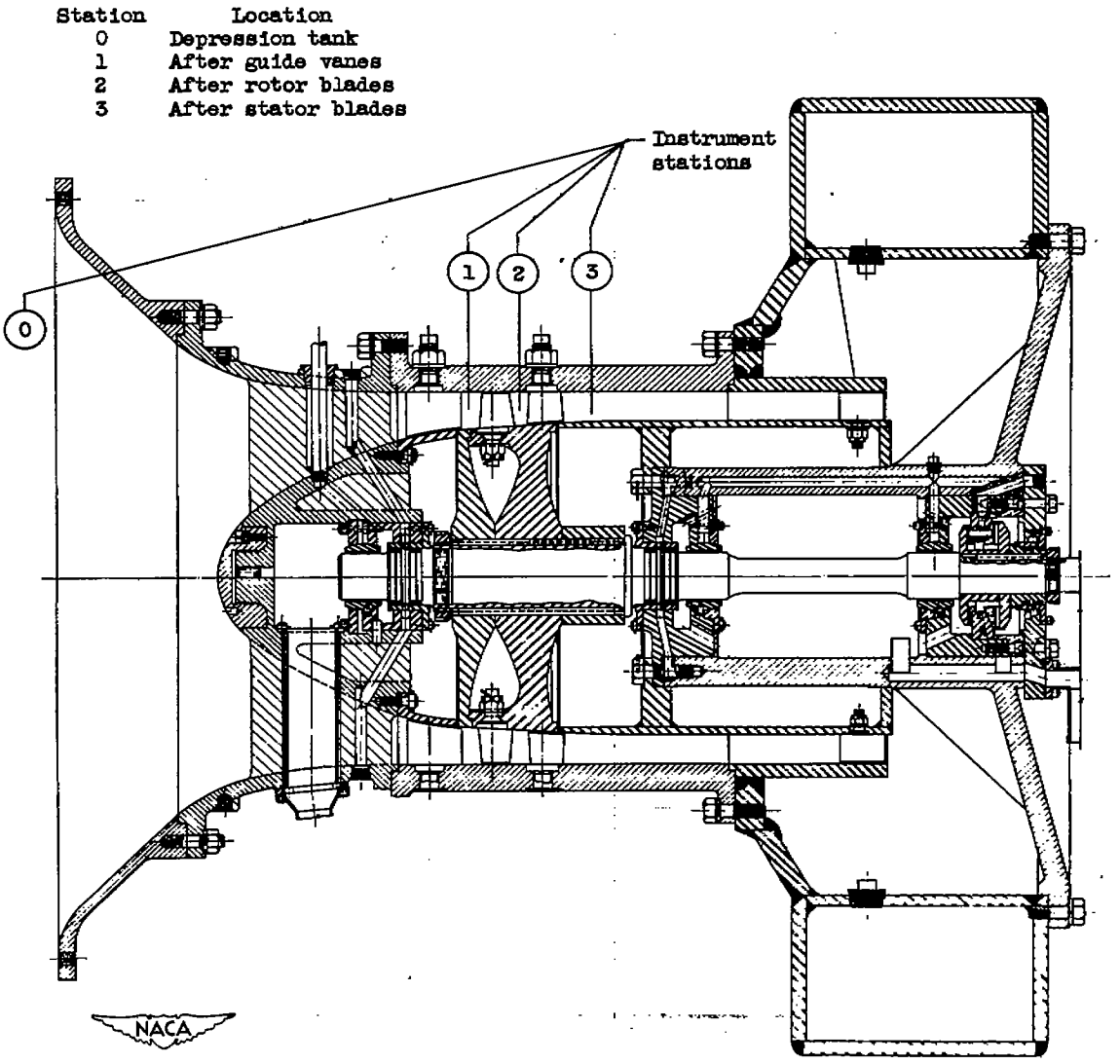

Figure 1. - Cross-sectional view of compressor showing instrument stations.

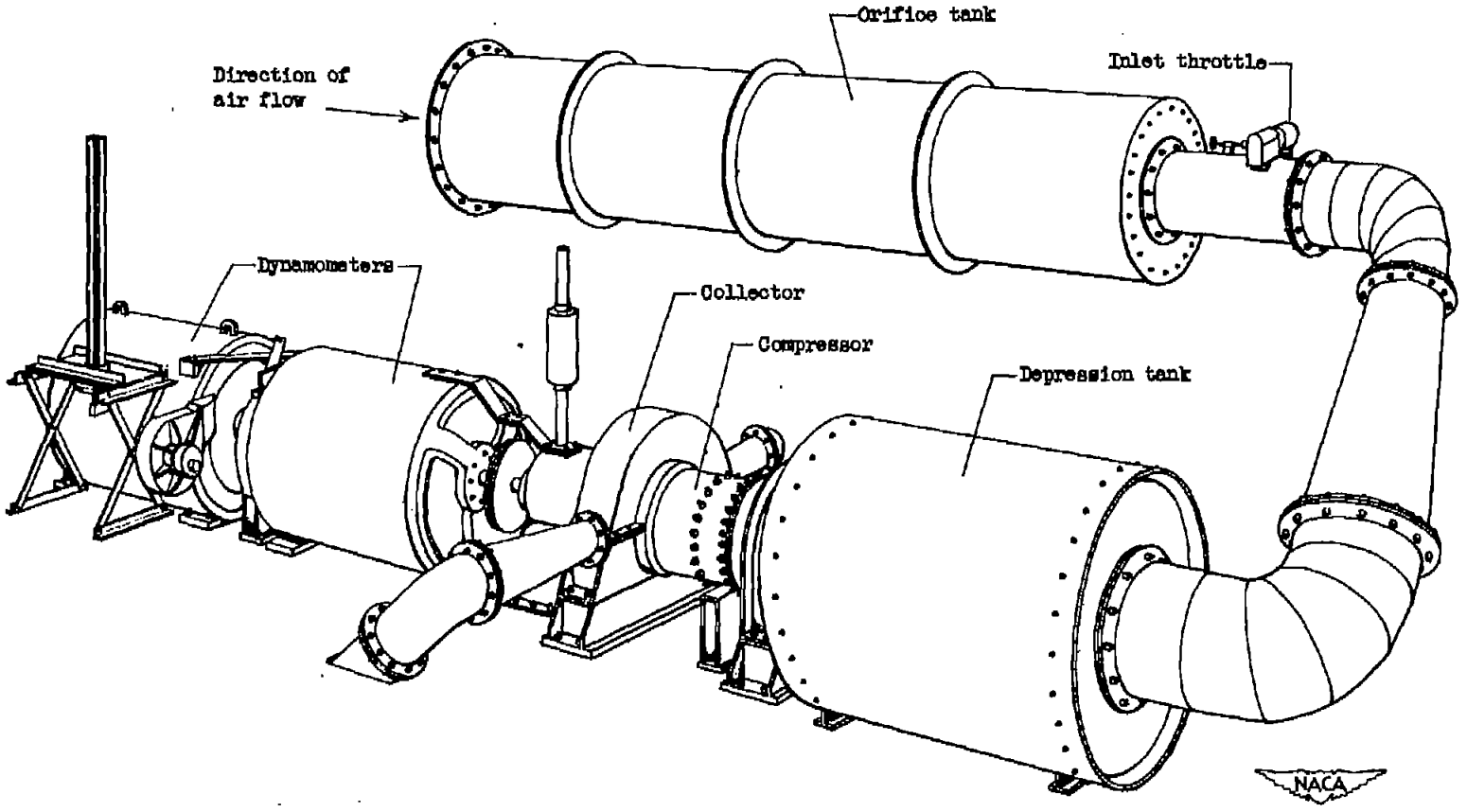

Figure 2. - Experimental setup for single-stage axial-flow compressor.

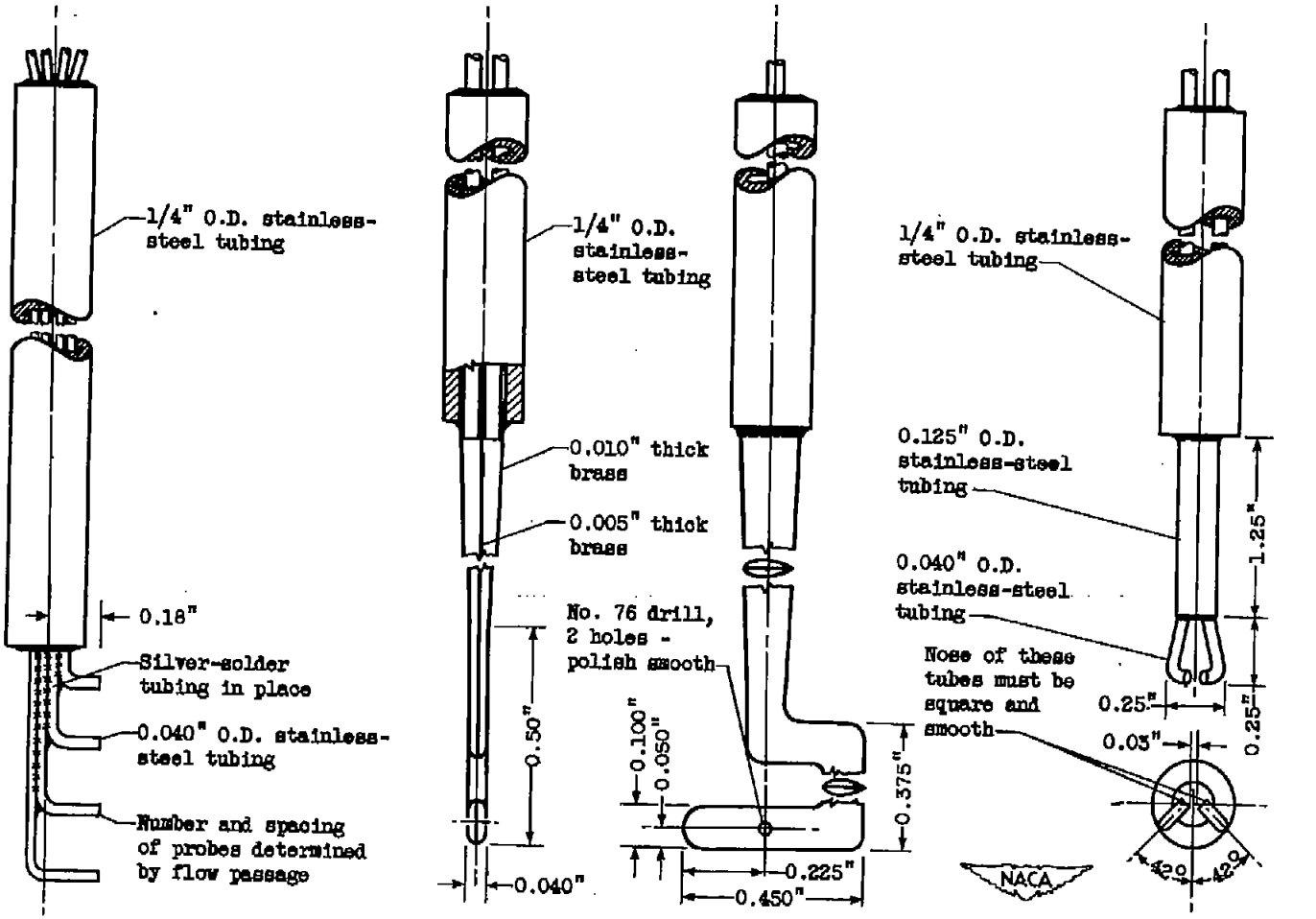

(a) Total-pressure rake. (b) Miniature static-pressure survey tube. (c) Claw survey tube.

Figure 3. - Instruments used in compressor-performance investigation.

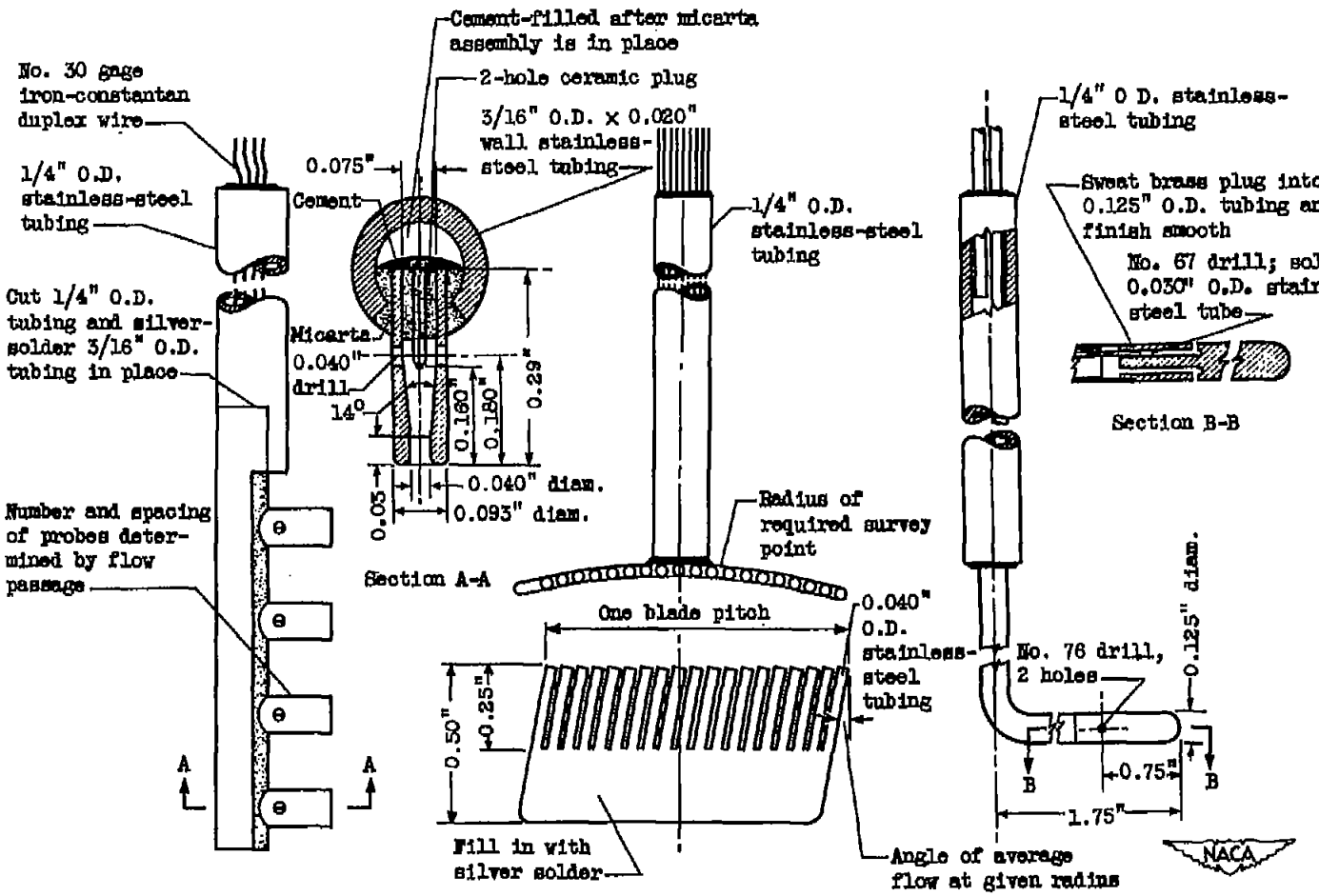

(d) Thermocouple rake. (e) Circumferential total-pressure rake. (f) Static-pressure survey tube.

Figure 3. - Concluded. Instruments used in compressor-performance investigation.

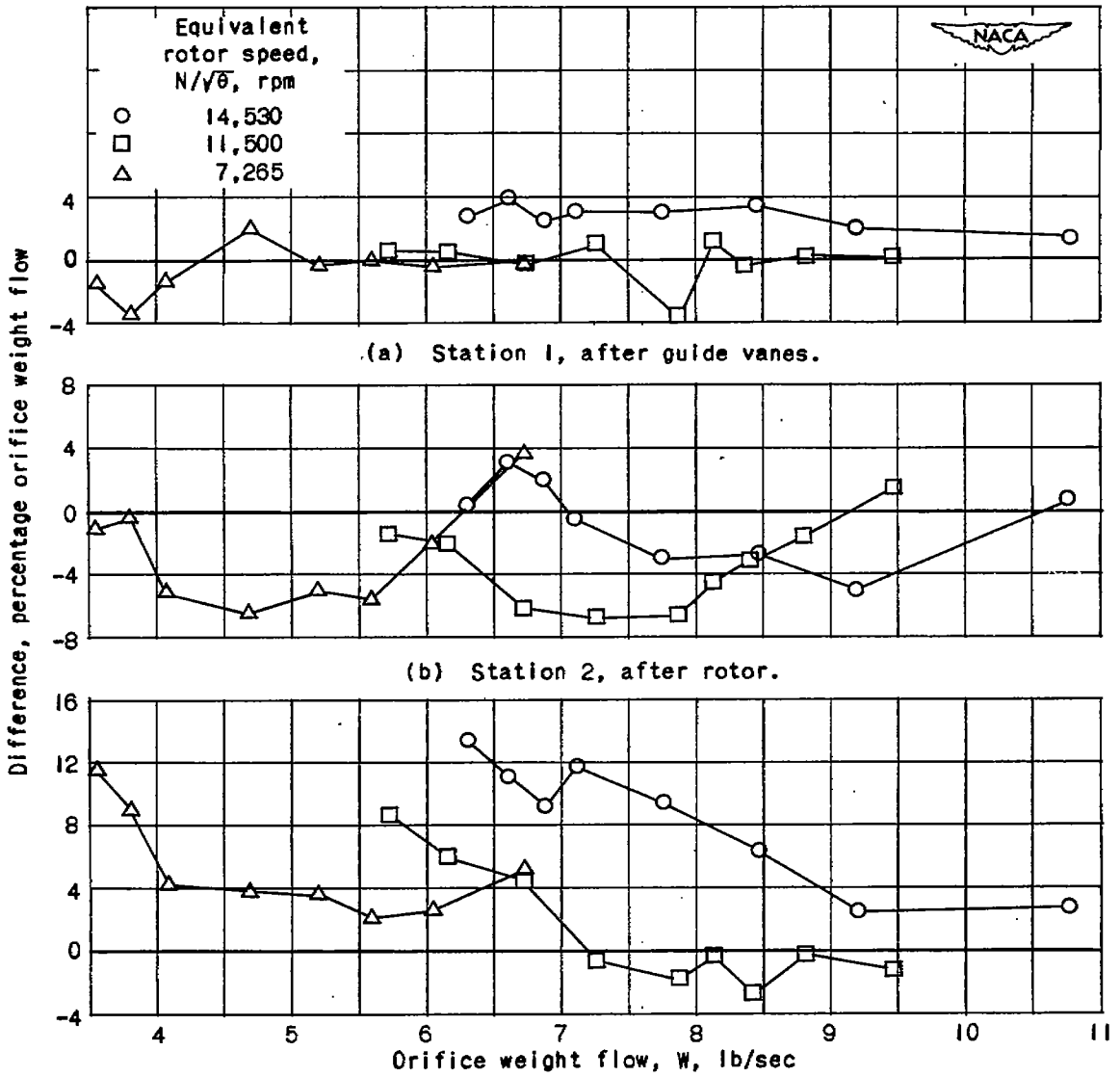

Figure 4. - Difference between integrated weight flows at three measuring stations and orifice weight flow expressed in percentage of orifice weight flow.

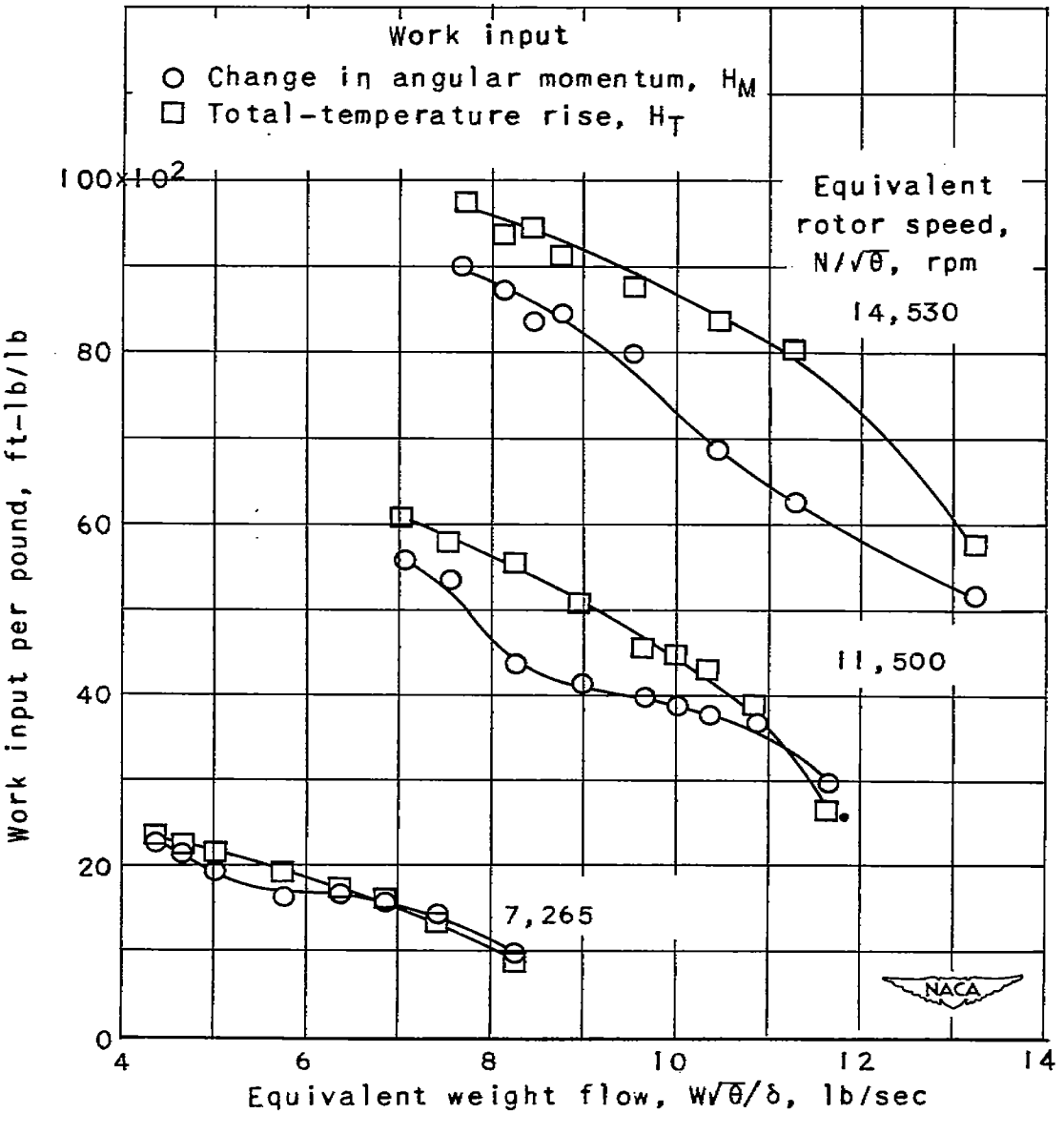

Figure 5. – Comparison of two methods of measuring work input to air.

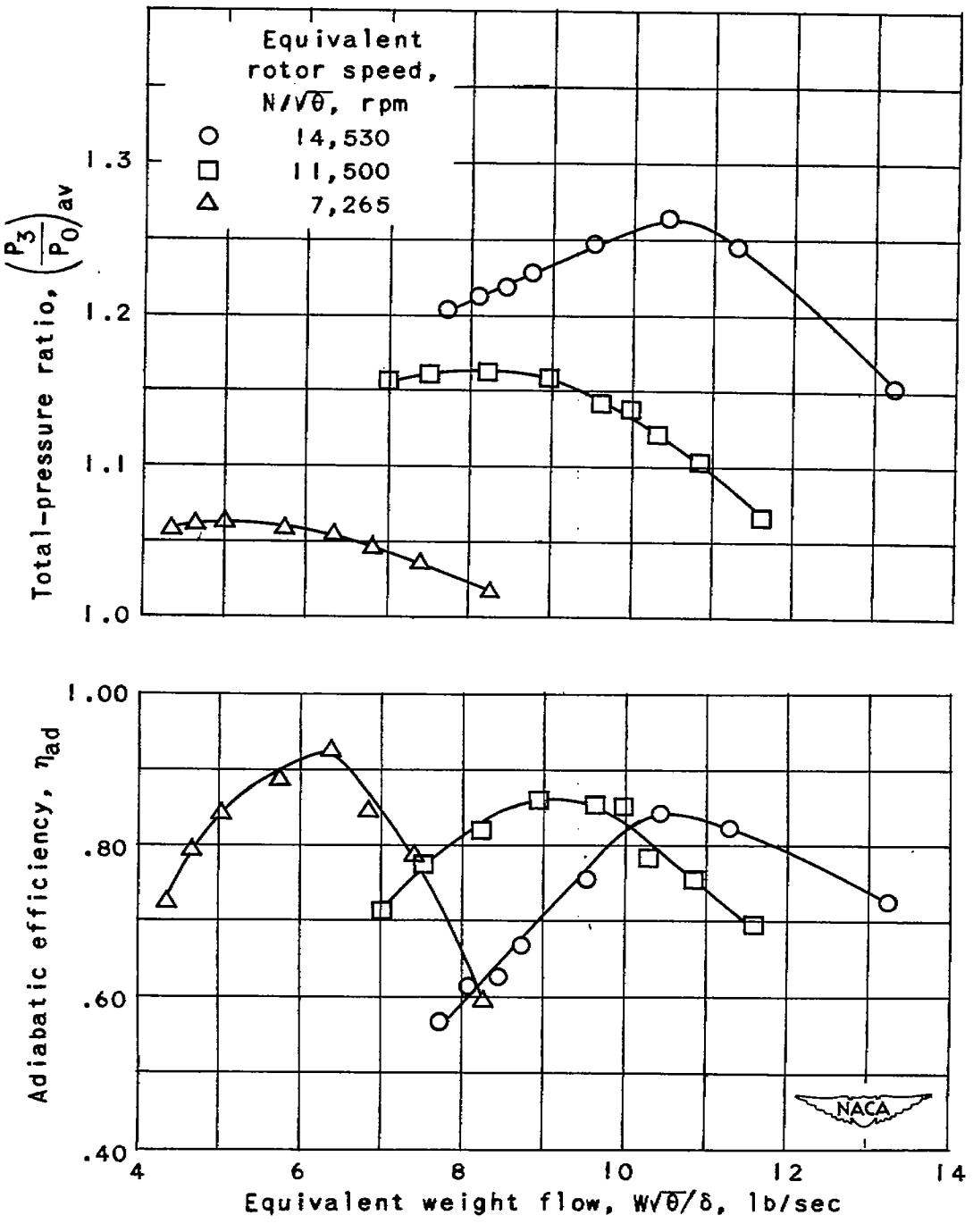

Figure 6. - Over-all performance of a 14-inch diameter single-stage axial-flow compressor using the NACA 5509-34 blade section.

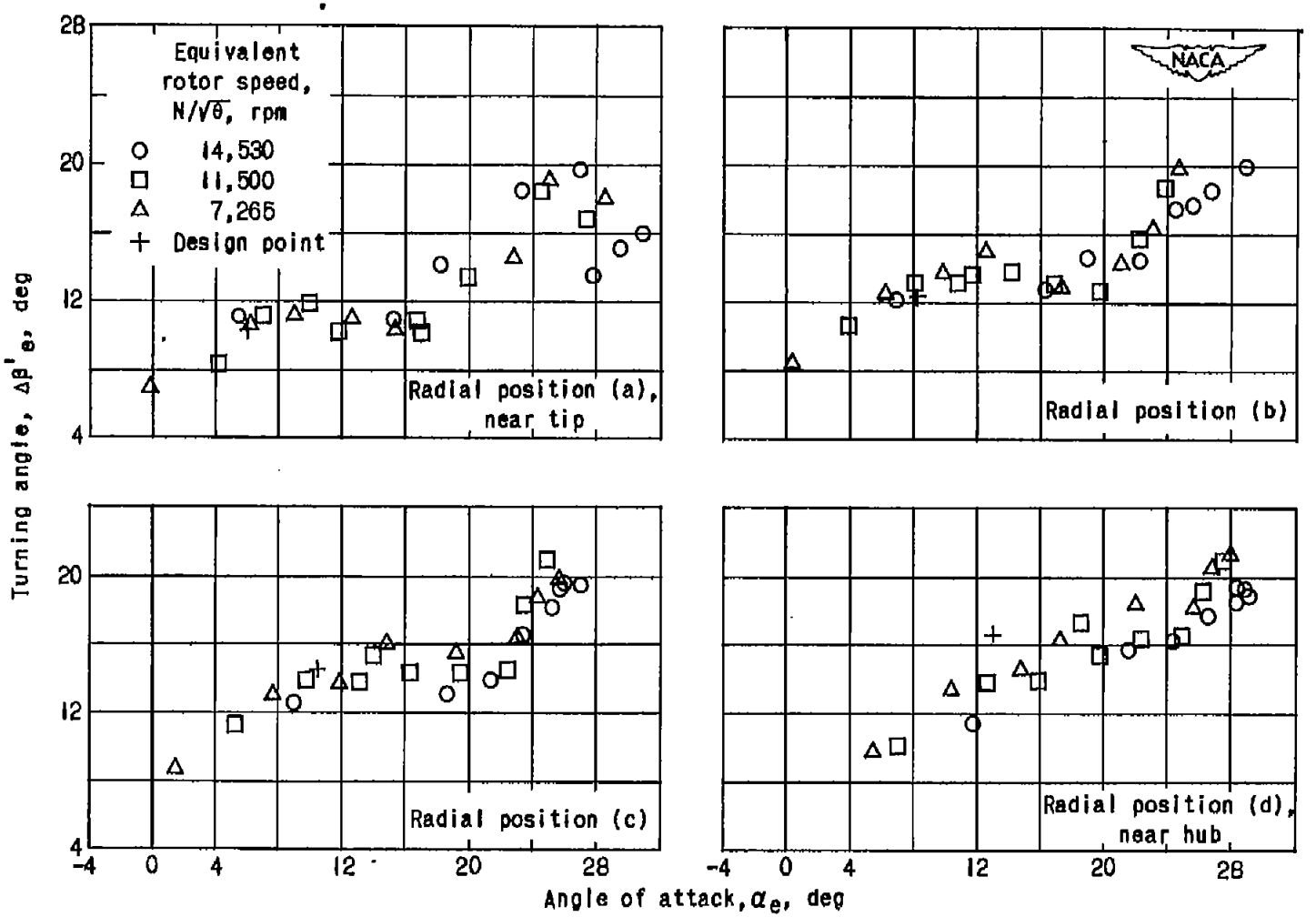

(a) Rotor.

Figure 7. - Variation of turning angle $\Delta\beta'_e$ with angle of attack α_e. NACA 5509-34 blade section.

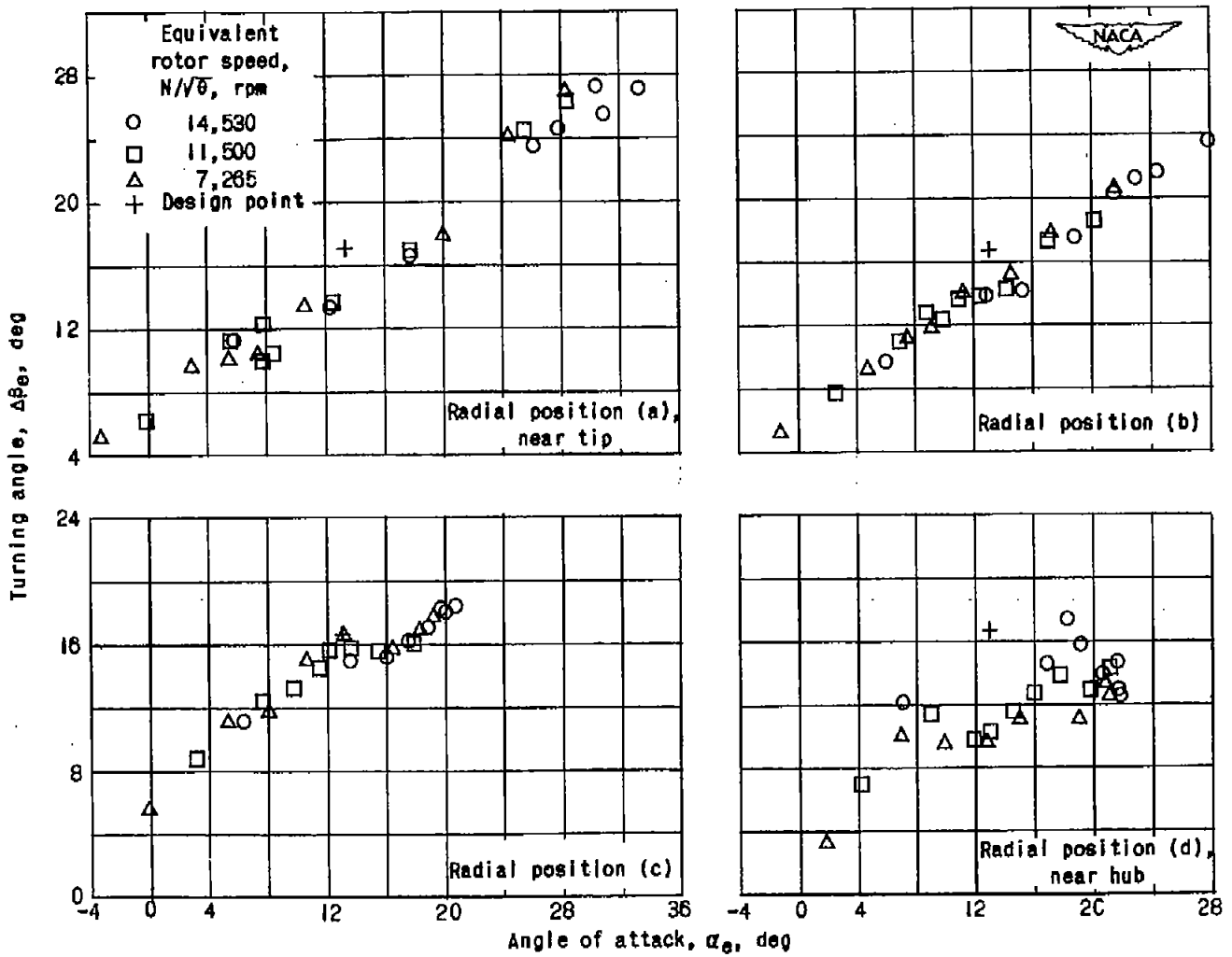

(b) Stator.

Figure 7. - Concluded. Variation of turning angle $\Delta\beta_e$ with angle of attack α_e. NACA 5509-34 blade section.

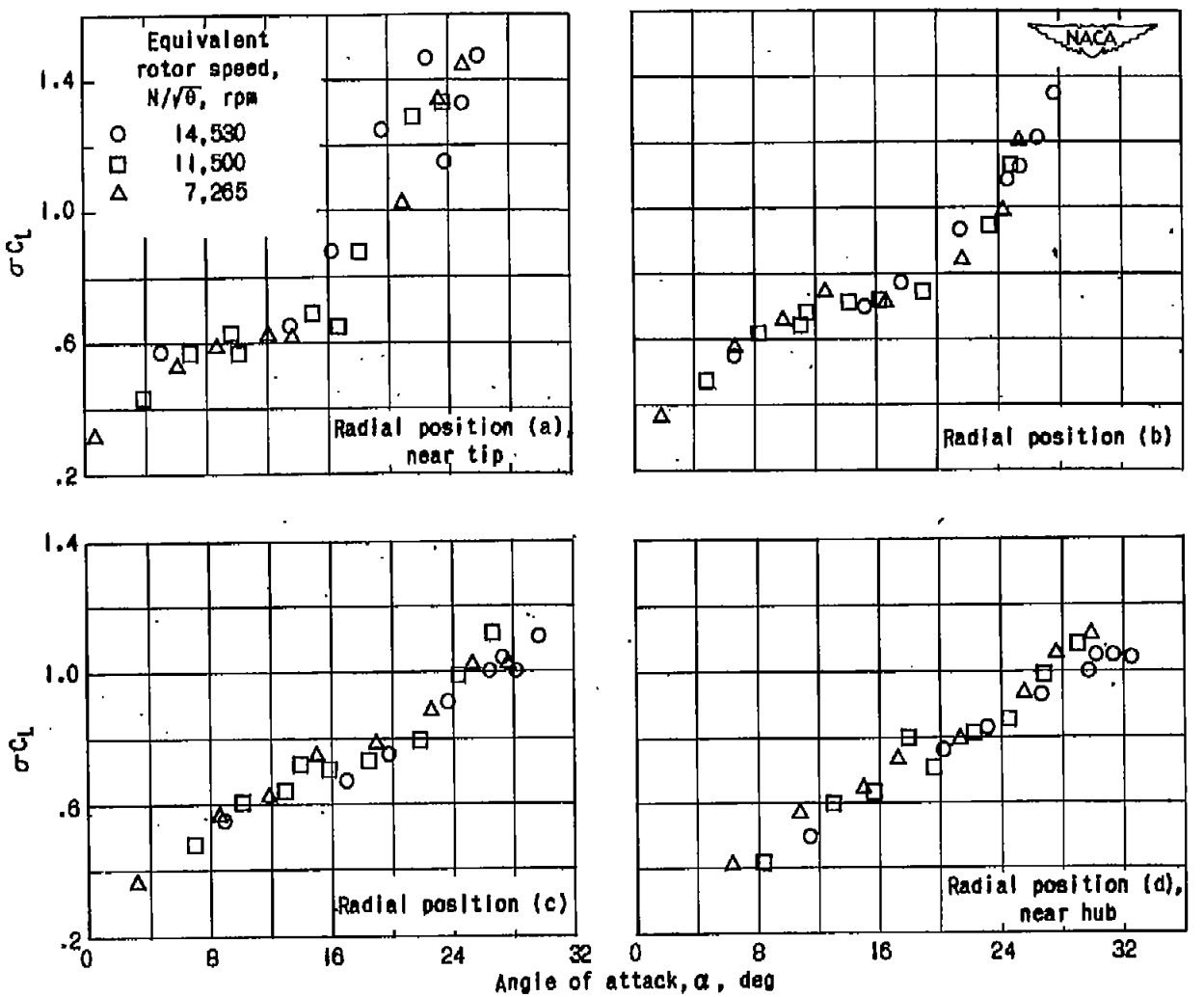

(a) Rotor.

Figure 8. - Variation of σC_L with angle of attack α. NACA 6509-34 blade section.

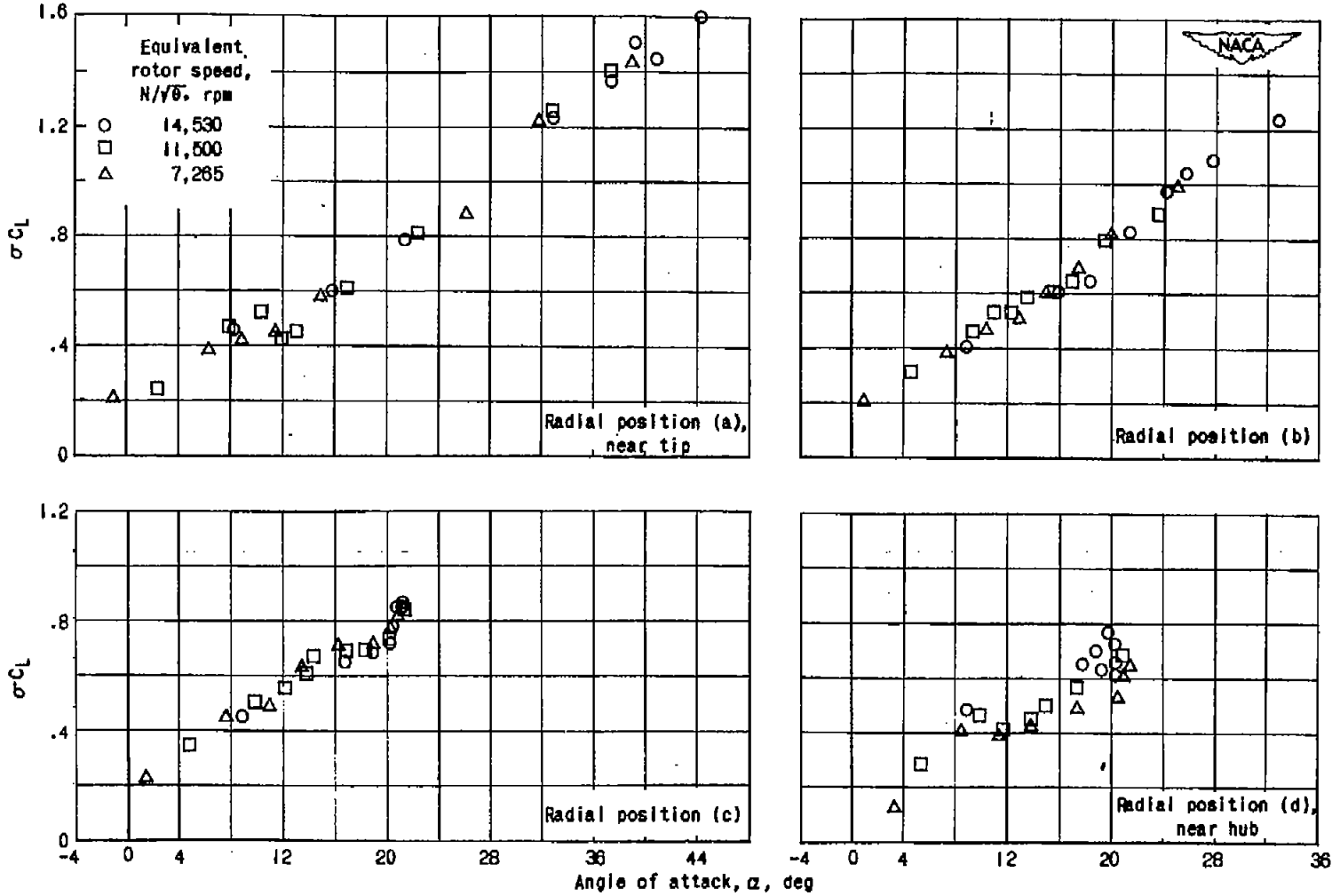

(b) Stator.

Figure 8. - Concluded. Variation of σC_L with angle of attack α. NACA 5509-34 blade section.

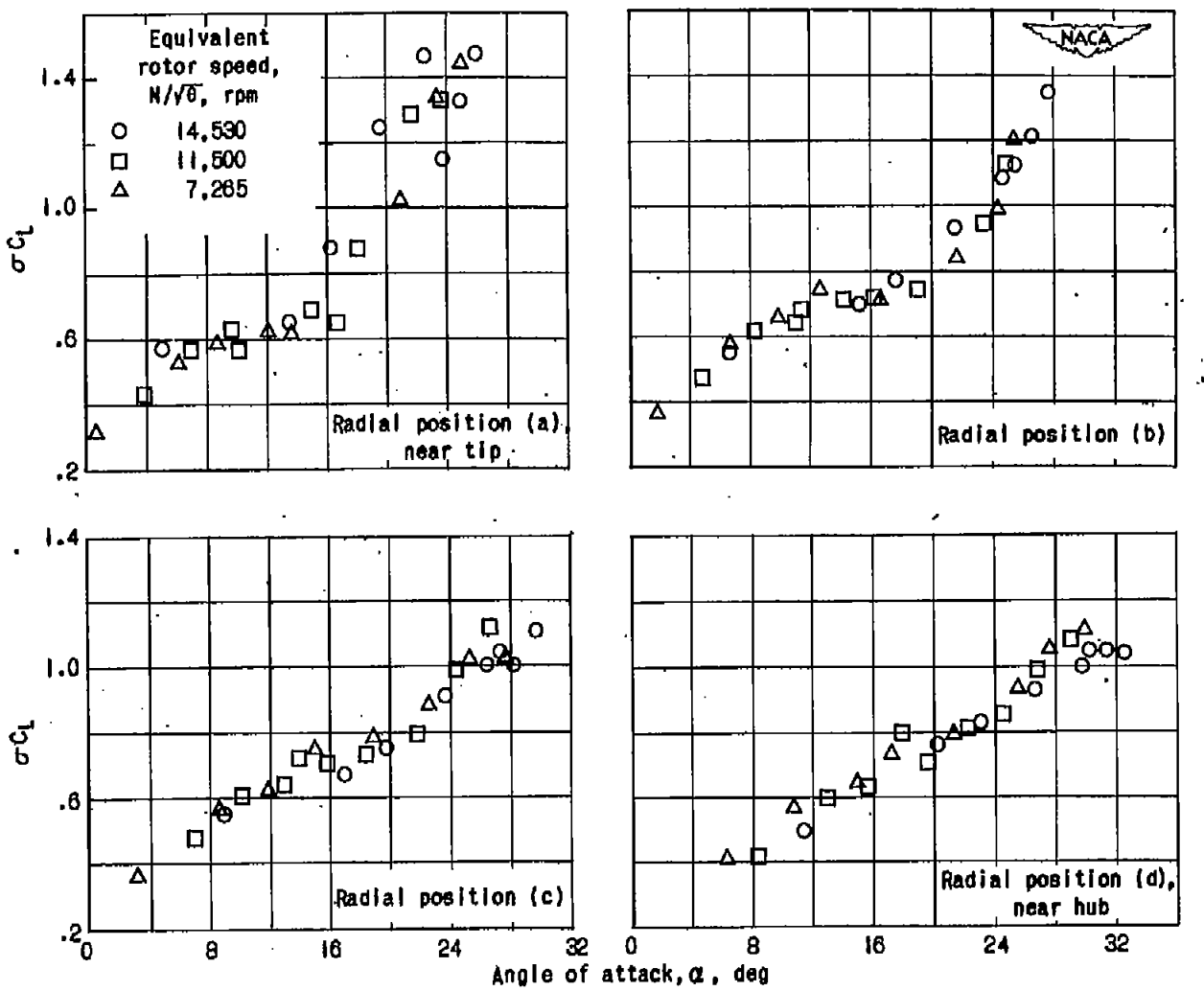

(a) Rotor.

Figure 8. - Variation of σC_L with angle of attack α. NACA 5509-34 blade section.

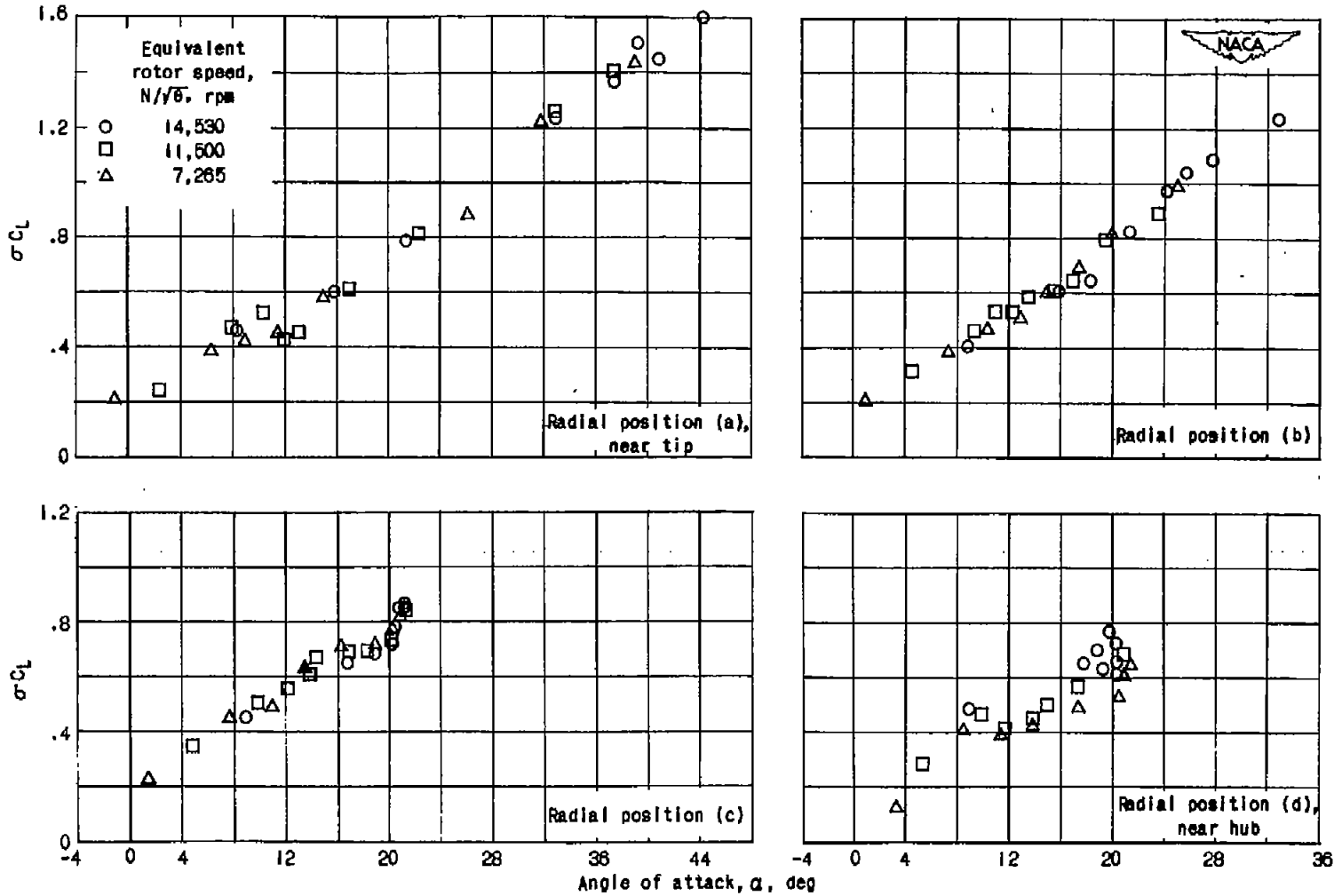

(b) Stator.

Figure 8. - Concluded. Variation of σC_L with angle of attack α. NACA 5509-34 blade section.

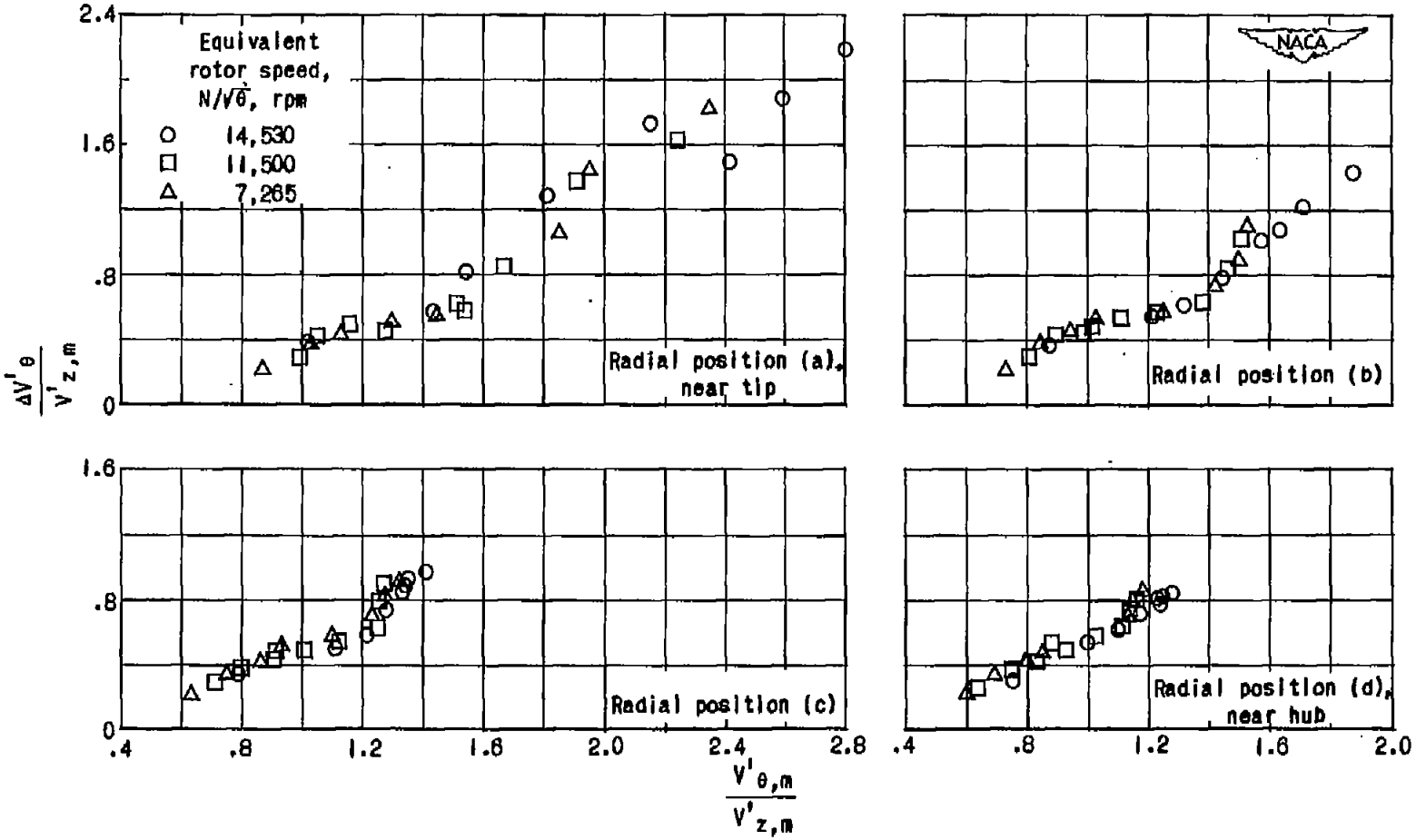

(a) Rotor.

Figure 9. - Variation of blade-loading parameter $\Delta V'_\theta/V'_{z,m}$ with $V'_{\theta,m}/V'_{z,m}$. NACA 5509-34 blade section.

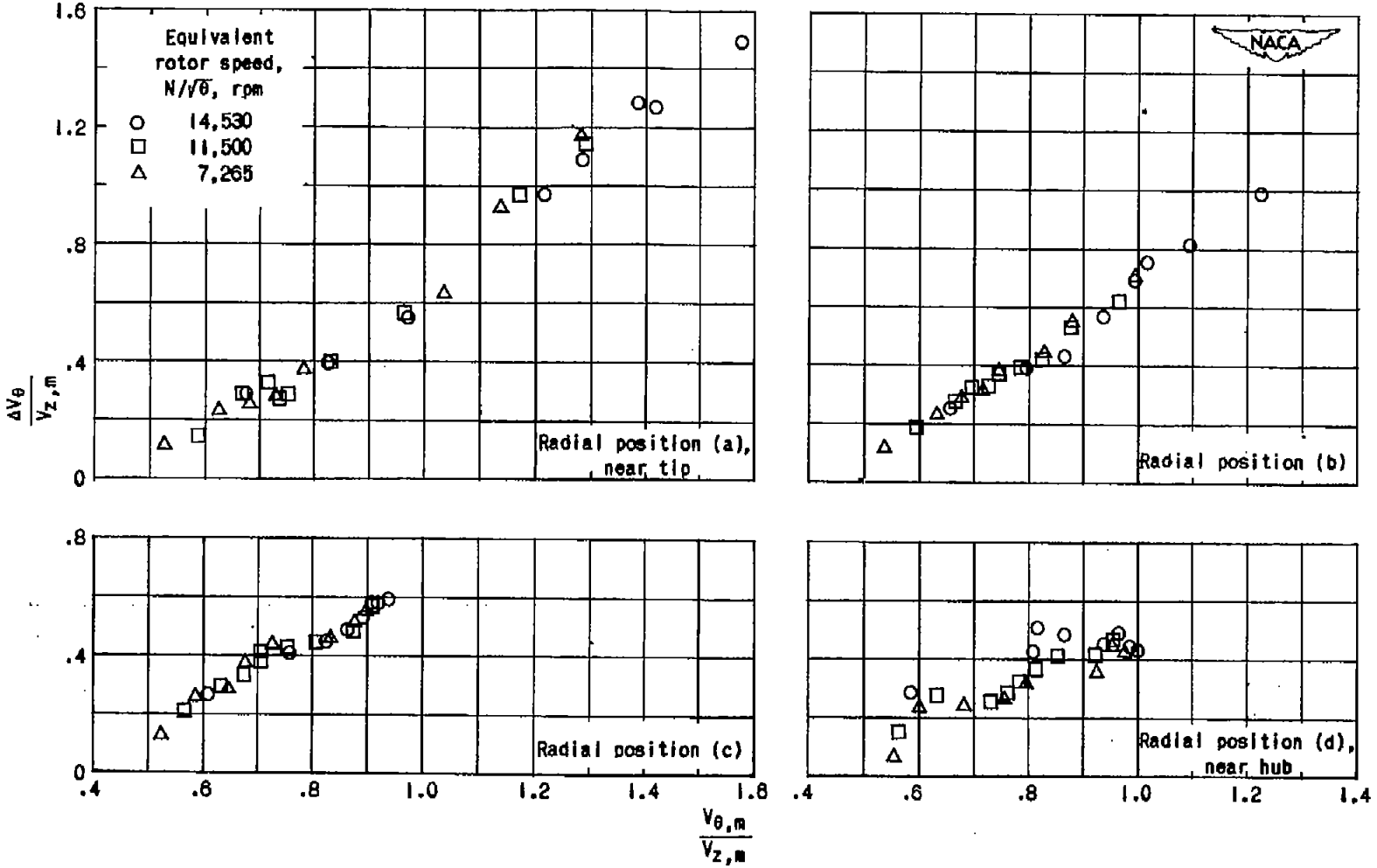

(b) Stator.

Figure 9. - Concluded. Variation of blade-loading parameter $\Delta V_\theta/V_{z,m}$ with $V_{\theta,m}/V_{z,m}$. NACA 5509-34 blade section.

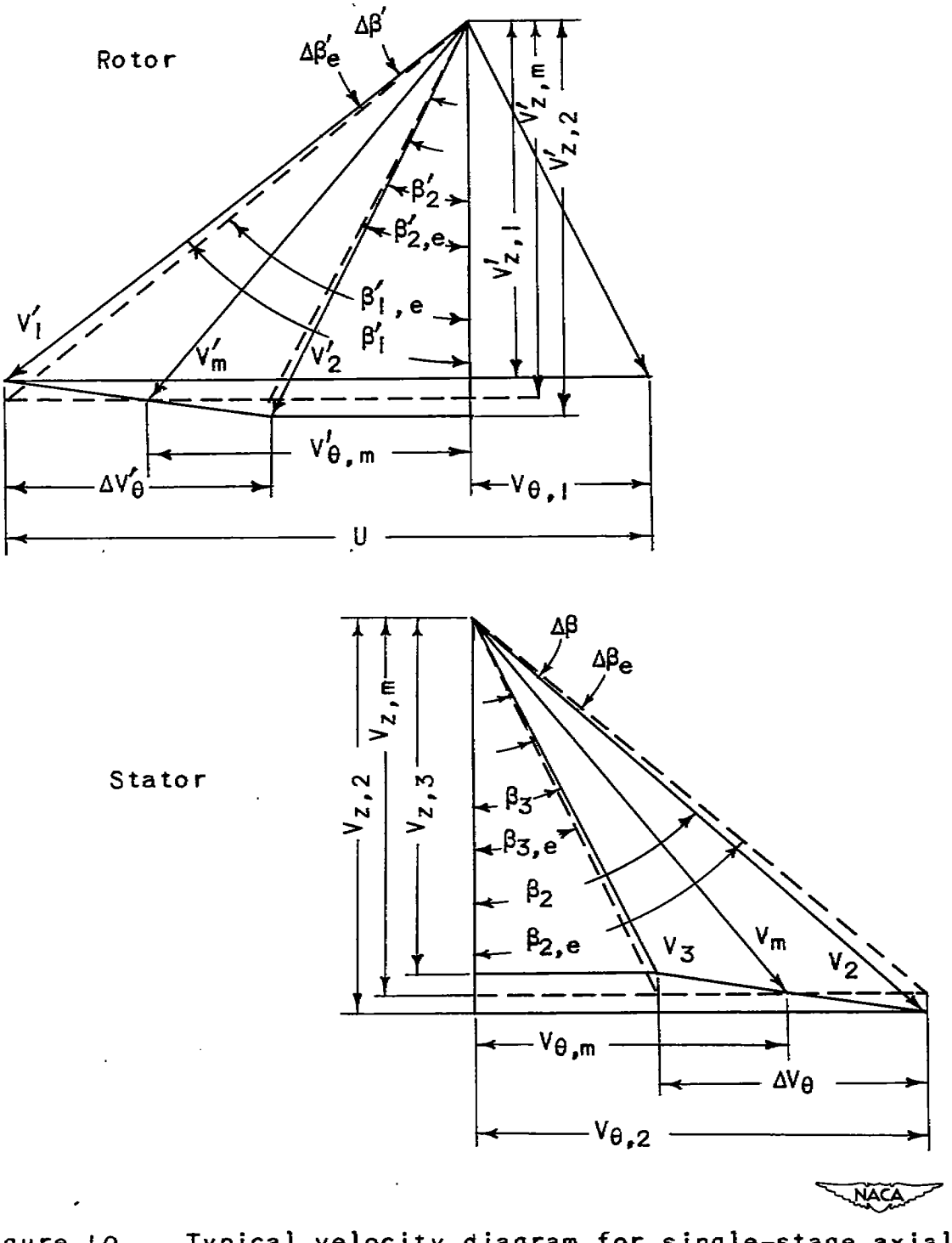

Figure 10. – Typical velocity diagram for single-stage axial-flow compressor.